NASA
Technical
Paper
3199

November 1992

Fracture Toughness Testing of Polymer Matrix Composites

Joseph E. Grady

NASA

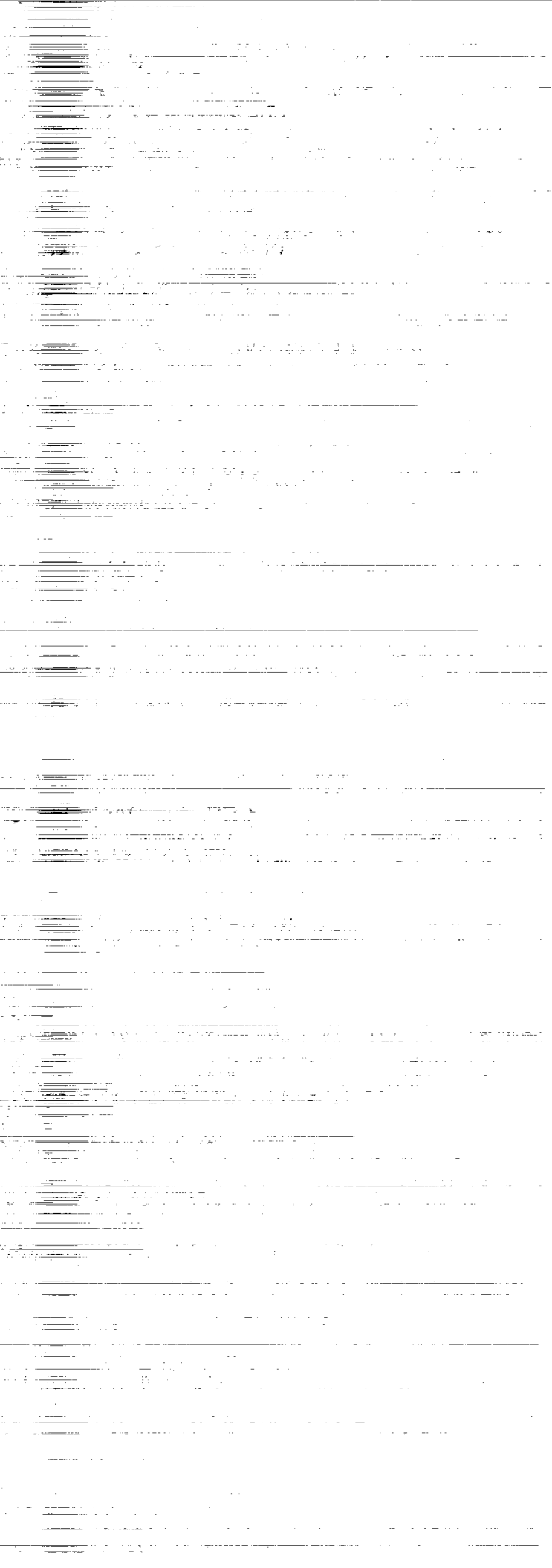

NASA Technical Paper 3199

1992

Fracture Toughness Testing of Polymer Matrix Composites

Joseph E. Grady
Lewis Research Center
Cleveland, Ohio

NASA
National Aeronautics and Space Administration
Office of Management
Scientific and Technical Information Program

Summary

A review of the interlaminar fracture literature indicates that a standard specimen geometry is needed to obtain consistent fracture toughness measurements in polymer matrix composites. In general, the variability of measured toughness values increases as the toughness of the material increases. This variability could be caused by incorrect sizing of test specimens and/or inconsistent data reduction procedures. A standard data reduction procedure is therefore needed as well, particularly for the tougher materials.

Little work has been reported on the effects of fiber orientation, fiber architecture, fiber surface treatment on interlaminar fracture toughness, and the mechanisms by which the fibers increase fracture toughness are not well understood. The little data that is available indicates that woven fiber reinforcement and fiber sizings can significantly increase interlaminar fracture toughness.

Introduction

The most common failure mode in laminated composite materials is interlaminar fracture, or *delamination* between laminate plies. In this report, the experimental methods and associated data analysis techniques used to measure the resistance to interlaminar fracture, or *fracture toughness*, of polymer matrix composite materials are described. A brief background in the use of energy methods to characterize fracture in elastic solids is given first. This serves as the basis for the explanations of fracture toughness tests and failure criteria presented later. In the following sections, rate-dependent fracture behavior is discussed and an overview of the various approaches used in the design of delamination-resistant composite materials is also given. Symbols are defined in appendix A.

Fracture Mechanics Background

In this section, criterion for interlaminar fracture are given, and the various modes of fracture are illustrated.

Fracture Criterion

An elastic body under an applied load satisfies the energy balance (refs. 1 and 2):

$$W = U + T + D \tag{1}$$

where

W = external work done by applied loads

U = strain energy

T = kinetic energy

D = energy dissipated through fracture

A fracture of the structure causes an increase in crack surface area, as shown in figure 1. The fracture also causes changes in external work, strain energy, kinetic energy, and fracture energy such that the energy balance condition (1) remains satisfied:

$$\Delta W = \Delta U + \Delta T + \Delta D \tag{2}$$

If the fracture resistance R of material is defined as the energy dissipated in the process of generating a unit of new crack surface area,

$$R = \frac{\Delta D}{\Delta A} \tag{3}$$

and the energy release rate G is

$$G = \frac{\Delta W}{\Delta A} - \frac{\Delta U}{\Delta A} \tag{4}$$

then from equations (2) to (4) we have

$$G - R = \frac{\Delta T}{\Delta A}$$

so the rate at which the cracked structure gains kinetic energy is determined by the amount of excess crack driving force (G - R). Under static loading conditions, the kinetic energy due to fracture is negligible, and the energy balance at fracture can be taken as

$$G - R = 0$$

Fracture can therefore occur when the energy release rate is equal to the fracture resistance of the material. If the critical energy release rate G_c is defined as the fracture resistance of the material, fracture occurs when the energy release rate reaches this critical value: $G = G_c$. The critical value G_c is the fracture toughness of the material.

Compliance Method

Energy conservation principles can also be used (ref. 2) to express the energy release rate in terms of the applied loading

and elastic material properties of the cracked structure. This approach gives the following result:

$$G = \frac{P^2}{2B}\frac{dC}{da} \qquad (5)$$

where a is the crack length and B is the crack width, as shown in figure 1, and P is the applied load. The compliance C of the cracked structure is given by

$$C \triangleq \frac{\delta}{P}$$

where δ is the displacement at the loading point.

Fracture Modes

A crack can propagate in any combination of the three modes shown in figure 2. A mode I fracture is driven by the crack-opening action from the normal stress, σ_y, perpendicular to the crack plane. A shearing stress, σ_{xy}, parallel to the fracture plane will cause the crack to propagate with a mode II (in-plane shearing) deformation, and the shearing stress, σ_{xz}, will drive a mode III (out-of-plane shearing) crack extension. Experimental measurements have shown that the fracture resistance of most materials depends on the mode of loading at the crack tip. Therefore, separate material properties G_{Ic}, G_{IIc}, and G_{IIIc} are needed to characterize the fracture toughness of a particular material under different loading conditions. Below, a series of test methods and data reduction procedures is described for measuring interlaminar fracture toughness of polymer matrix composites under mode I, mode II, and mixed mode I-mode II loading.

Interlaminar Fracture Tests and Data Reduction Procedures

Mode I Loading

The Double Cantilever Beam (DCB) specimen was originally used to measure the toughness of adhesive bonds between metals (ref. 3). Since then it has been modified for use as a mode I interlaminar fracture-toughness test specimen for composites. A typical composite DCB specimen is shown in figure 3(a). The delamination is usually initiated from an embedded notch by placing a thin, nonadhesive film between two of the plies during layup (ref. 5). This prevents those plies from bonding in that area during the cure cycle and creates an initial delamination, as shown in figure 3(b).

If the two arms of the DCB specimen are considered to be beams cantilevered at the crack tip, the elastic compliance is given from simple beam theory as

$$C(a) = \frac{\delta}{P} = \frac{8a^3}{EBh^3} \qquad (6)$$

where E is the flexural modulus of the two cantilevered arms (ref. 6) and the other parameters are as defined in figure 3(b).

The energy release rate for the DCB specimen is given from equation (5) as

$$G_I = \frac{12P^2a^2}{EB^2h^3} \qquad (7)$$

This is called the beam model of the DCB test specimen.

Crack Tip Compliance

Several modifications to the beam model have been used to more closely model the actual deformation of the DCB test specimen. The first modification accounts for the flexural compliance at the crack tip.

The arms of the DCB test specimen are not rigidly clamped at the crack tip, as assumed in the beam model. In fact, there can be a rotation (θ) about the z-axis and a transverse displacement (δ) of the crack tip due to the compliant restraint. The assumption of a "fixed" boundary may therefore be more closely satisfied ahead of the actual crack tip, at some point where the rotation and displacement are negligible. An "effective crack length" (ref. 7) given by

$$a_{eff} = a + a^*$$

is therefore used in equation (6) to account for the compliance at the crack tip. The correction term a^* is usually expressed in terms of the thickness, t, of the interply layer:

$$a^* = \beta t$$

where β is a constant chosen to match equation (6) with the measured compliance data. A value of $\beta = 0.37$ was used for DCB tests of adhesive bonds (ref. 7), but similar tests of stiffer graphite-epoxy composites (ref. 8) found β to be negligible.

Shear Compliance

In highly orthotropic materials such as those considered here, there may be a significant amount of transverse shear deformation because the shear modulus is usually much lower than the in-plane moduli. When shear compliance is considered, the total compliance of the DCB test specimen is given (ref. 6) by

$$C(a) = \frac{8a^3}{EBh^3}(1 + S)$$

where S is the shear correction factor:

$$S = \frac{3}{10}\frac{E}{G_{13}}\left(\frac{h}{a}\right)^2$$

and G_{13} is the transverse shear modulus, which is equal to the in-plane shear modulus G_{12} if the composite material is assumed to be transversely isotropic. In this case, the energy release rate is

$$G_I' = \frac{12P^2}{EB^2h}\left[\left(\frac{a}{h}\right)^2 + \frac{1}{10}\frac{E}{G_{13}}\right] \qquad (8)$$

The relative contribution of the shear term in equation (8) is expressed in terms of the crack length and material orthotropy ratio, E_1/E_2 in references 6 and 9. The shear correction increases the energy release rate by approximately 10 percent for a highly orthotropic material such as graphite/epoxy (E_1/E_2 = 14) when the crack length is relatively short (a/h = 17). As shown in figure 4, the effects of shear compliance decrease for longer crack lengths and lower orthotropy ratios.

Large Displacements

If the compliance of the DCB specimen is too high, the linear elastic analysis described in this section may be inadequate to model the large displacements and rotations that occur under loading. A nonlinear elastic model of a cantilevered composite beam was therefore developed (ref. 10), as shown in figure 5, to account for arbitrarily large displacements. The deformation of the cantilevered arms (and the resulting energy release rate) deviates significantly from that calculated using linear beam theory (fig. 6) for relatively large ($\delta/a > 0.3$) displacements.

Data Reduction Procedures: DCB Specimen

Load-displacement test data typical of a uniform DCB made from a brittle epoxy matrix composite are shown in figure 7. Multiple cycles are shown of loading, stable crack propagation, and arrest, followed by elastic unloading. The unloading should always be elastic; that is, the displacement should return to zero when the load is removed. Permanent deformation indicates that failure mechanisms other than interlaminar fracture have contributed to the energy dissipated by the structure during loading cycle, and therefore result in an erroneously high calculation of fracture toughness. This section presents several different techniques for determining the fracture toughness from load-displacement data like that shown in figure 7.

Beam analysis method. – The effects of transverse shear deformation and large displacements can be minimized by careful design of the DCB specimen. If these effects do not contribute significantly to the deformation of the test specimen, the simple beam model can be used to calculate the mode I fracture toughness G_{Ic} from load-displacement data such as those shown in figure 7. This approach is called the beam analysis method. Combining equations (6) and (7), we have (ref. 4)

$$G_I = \frac{3}{8B}\,\frac{P\delta}{a} \tag{9}$$

The mode I fracture toughness of the composite is therefore given by

$$G_{Ic} = \frac{3}{8B}\,\frac{P_c\delta_c}{a_c} \tag{10}$$

where P_c is the critical applied load that produces a separation δ_c of the cantilevered arms and causes the existing delamination of length a_c to extend. This expression is more useful than equation (7) for estimating fracture toughness from test data for two reasons. The flexural modulus, E, does not have to be estimated, either from test data or analysis; and the a^2 term is eliminated, thereby reducing the error in G_{Ic} for a given error in crack length measurement.

Thus the fracture toughness can be determined by measuring load, displacement, and crack length during a DCB test. A typical configuration for a DCB test is shown in figure 8.

Compliance calibration method. – The empirical-based data reduction scheme described here was first used to measure the fracture toughness of unreinforced polymers (ref. 13) and later applied to composites (refs. 5 and 14). In this approach, the measured compliance is assumed to be of the more general form

$$C(a) = \frac{a^n}{K}$$

where the constants n and K are determined by curve-fitting a plot of log (C) versus log (a). The energy release rate, from equation (5), is then

$$G_I = \frac{nP\delta}{2Ba}$$

This approach has an advantage in that it does not inherently assume that the beam bending model determines how the compliance varies with crack length. The effects of shear deformation, crack tip compliance, and/or large displacements will change the overall compliance of the test specimen and therefore will be accounted for automatically by the calculated curve-fit parameters, n and K.

Area method. – A single load-crack extension-unload cycle for a brittle matrix composite DCB specimen is shown schematically in figure 9. The applied load is increased until a load of P_1 is reached, which causes an existing crack (delamination) of length a_1 to extend. When the crack reaches length a_2, its propagation is arrested. Because of the crack extension, the load drops to P_2 and the load point displacement increases to δ_2. The applied load is then removed. The area between the loading and unloading curves, designated ΔA, represents the decrease in stored strain energy caused by the crack extension. Given that the distance Δa that the crack extended because of the load is

$$\Delta a = a_2 - a_1$$

then,

$$G_c = \frac{\Delta A}{B\Delta a} \tag{11}$$

is the critical strain energy release rate required to cause crack extension, where $(B\Delta a)$ is the amount of new crack surface area generated by the crack extension. For the brittle fracture behavior depicted in figure 9, equation (11) can be approximated (ref. 4) by

$$G_c = \frac{P_1\delta_2 - P_2\delta_1}{2B\Delta a} \tag{12}$$

The advantage of this method is that fracture toughness is calculated from the difference in area between the two load-displacement curves (i.e., before and after crack extension). There is no requirement for the load-displacement curve to be linear. Therefore, equation (11) can be generalized for materials

that have nonlinear elastic load-displacement curves, such as a composite material with a toughened (and therefore more ductile) matrix, like that shown in figure 10. In this case, however, the simplification made in equation (12) for the linear case is not applicable, and a numerical integration scheme may be required to calculate the area between the loading and unloading curves.

J-integral method. — The fracture energy released from a DCB specimen with a nonlinear load-displacement curve is shown in figure 10(a). If loading caused a permanent deformation, the area method would overestimate the material's toughness (fig. 10(b)). A different means of calculating the energy released due to fracture is therefore required when permanent deformation occurs in the material. The J-integral (ref. 15) is a measure of the energy available for crack extension and can be applied even when irreversible deformation occurs. For elastic deformation, the J-integral has the same value and meaning as the energy release rate; that is, $J = G$ for elastic deformation. An empirical method of calculating J for fracture-toughness testing is given in reference 12 and outlined in figure 11. In step 1, load-displacement curves are plotted for successive delamination lengths, $a_1 < a_2 < a_3$. The strain energy U is then calculated by integrating these curves:

$$U(\delta) = \int_0^{\delta} P(\zeta)d\zeta$$

and plotted; curve fitting is used to smooth the data. The J-integral is then calculated by differentiating the smoothed data

$$J = -\frac{1}{B}\frac{dU}{dA} \qquad (13)$$

as shown in step 3. The fracture toughness of the material J_{Ic} is the value of J obtained by evaluating equation (13) at the critical displacement δ_c, just before crack extension occurs.

Design Considerations: DCB Specimen

In this section, guidelines are provided for the effective design of a mode I fracture-toughness test and for a physically meaningful interpretation of the test results. Included are guidelines for choosing ply orientations and dimensions of the DCB test specimen based on the collective results previously presented.

Hinged loading. — If the loading is applied to the test specimen through hinges adhesively bonded to the cantilevered arms (fig. 12), the bending moment caused by over-restraining the arms is eliminated (ref. 16), thereby leaving the arms free to rotate during loading. For this configuration, the effective delamination length (a) and specimen length (L) are defined from the location of the hinge.

Tapered width. — The width-tapered DCB specimen shown in figure 13 was designed to maintain a constant fracture load as the crack length increases (ref. 18). The compliance of the width-tapered DCB is given by equation (6); however, the specimen width B increases linearly along the span;

$$B = ka$$

where a denotes the crack length and k is the taper ratio. The test specimen compliance is therefore given by

$$C(a) = \frac{8a^2}{Eh^3}\frac{1}{k}$$

and the energy release rate, from equation (5), is

$$G_I = \frac{8P^2}{Eh^3}\left(\frac{1}{k}\right)^2$$

which is independent of crack length. The critical load P_c required to cause crack extension is therefore independent of crack length. Similar results have been achieved (refs. 18 and 19) using DCB specimens tapered in the thickness direction.

Ply orientation. — For several reasons, DCB test specimens are generally constructed from unidirectional 0° plies. High bending stiffness can minimize large deflections and resulting analytical complexities. In addition, the delamination tends to follow the 0° plies (ref. 20) and grow in a self-similar manner at a 0°/0° interface. This is not necessarily true in laminates with multiple ply orientations (ref. 21) where the delamination may "wander" between several ply interfaces during loading and therefore violate the assumption of self-similar crack propagation required to apply a Linear Elastic Fracture Mechanics (LEFM) analysis. This can result in erroneously high measurements of apparent fracture energy (ref. 21). To minimize the tendency for the delamination to wander between ply interfaces in multiple ply orientations, symmetry should be used in the specimen design. The delamination should be located at the specimen midplane, and the layup should be symmetric about the midplane. In addition, the DCB cantilevered arms should be symmetric about their respective midplanes to avoid any twisting that would otherwise occur during loading (ref. 20) and divert the crack path.

Another factor to consider when choosing the ply orientations is the fiber-bridging effect on the fracture resistance of toughened-matrix composites. When a delamination grows between two 0° plies, individual fibers can bridge the delamination (fig. 14) and significantly increase the material's apparent fracture toughness (refs. 22 to 24). This occurs in part because the fibers of similarly oriented plies can nest together and migrate into the neighboring ply when pressure is applied during the cure cycle. The material shows an increasing resistance to fracture, or R-curve behavior, as the delamination grows and the bridged zone develops. Although this is a beneficial characteristic in practical applications of composite materials, it is undesirable in fracture toughness testing because the apparent fracture toughness of the material will vary with delamination length, fiber volume ratio, and test specimen geometry.

The fracture toughness data shown in figure 15 were measured from a unidirectional C6000/Hx205 DCB specimen with the delamination at the 0°/0° interface along the midplane (ref. 23). The fiber-bridging zone developed as the crack extended, tripling the initial fracture resistance of the material before reaching a plateau at a crack length of 100 mm. The fiber

nesting across the delamination was then eliminated by orienting the two plies on either side of the delamination at small angles to each other so that the fibers from the two plies could not migrate across the ply interface during the cure cycle. Although the amount of fiber bridging, and the resultant R-curve behavior, is significantly reduced, it is not completely eliminated. This was attributed (ref. 23) to the primary delamination linking with secondary flaws originated near a neighboring ply interface within the crack tip process zone (fig. 16). This type of fiber bridging is most likely to occur in composites with +toughened, and therefore more ductile, resins (ref. 26) because of the large process zone that develops near the delamination crack tip.

A significant decrease in R-curve behavior due to fiber bridging was noted when the thickness of the resin-rich interface layer was increased (ref. 24) and a thicker test specimen was used (ref. 27), this reduced the crack face separation and decreased the amount of load supported by the bridging fibers.

The following techniques can therefore be used to estimate the actual mode I fracture toughness of a composite material that develops significant amounts of fiber bridging:

(1) Reduce the amount of fiber nesting in the plies by using either of the two ply orientations discussed.

(2) Use a thicker test specimen.

(3) Use the initial measured values of G_c before a significant amount of fiber bridging develops.

For brittle-matrix composites, the mode I fracture toughness of the neat resin is a good estimate of the mode I interlaminar toughness of the composite (ref. 27) because of the small size of the process zone near the crack tip. However, the same is not true for the tougher resins (ref. 28).

Specimen thickness. – The beam theory model assumes a linear elastic deformation of the DCB specimen. The thickness of the specimen should therefore be chosen so that the displacements of the cantilevered arms remain linear elastic throughout the entire loading range, until fracture occurs. Equations (6) and (7) can be combined (ref. 29) to give

$$\frac{\delta_c}{a} = 4a\sqrt{\frac{G_{Ic}}{3Eh^3}}$$

where δ_c is the maximum displacement reached before crack extension. Since nonlinear displacements become significant for $\delta/a \geq 0.3$ (ref. 10), to maintain linear elastic behavior until fracture, the test specimen must be designed so that

$$4a\sqrt{\frac{G_{Ic}}{3Eh^3}} \leq 0.3$$

Given a maximum allowable crack length (a_*) for the test, this can be accomplished by choosing a sufficiently large value for specimen thickness, h. Solving for h gives

$$h^3 \geq \frac{16G_{Ic}a_*^2}{0.9E}$$

Thicker test specimens are therefore required for tougher materials (see fig. 17).

Initial crack length. – The effect of transverse shear varies with aspect ratio (a/h) and orthotropy ratio (E_1/E_2). Since crack extension increases the aspect ratio and decreases the contribution of transverse shear deformation to the overall compliance of the test specimen, shear compliance is greatest at the initial crack length. Therefore, choosing a long enough initial delamination will ensure that the effects of shear compliance are minimized over the entire range of crack lengths. For example, figure 4 shows that the simple beam theory would overestimate G_I by approximately 5 percent for a highly orthotropic material ($E_1/E_2 = 14$), with a crack aspect ratio (a/h) of 40, which corresponds to an initial crack length of approximately 2 in. for a 20-ply graphite-epoxy laminate.

Mode I fracture toughness measurements for a variety of different composites are given in table I in Appendix B.

Mode II Loading

The fracture resistance of composite materials is dependent on the loading mode. Interlaminar fracture toughness under mode II loading is usually much greater than that under mode I, particularly for brittle epoxy matrix composites. A separate mode II test is therefore required to characterize interlaminar fracture toughness. In contrast to mode I loading, no single test specimen geometry is universally used to measure G_{IIc}. The two most commonly used tests for mode II fracture toughness measurements are the end-notched flexure test and the end-loaded split test.

End-Notched Flexure Test

The end-notched flexure (ENF) specimen (fig. 18) is the geometry most frequently used to produce pure shear loading at the delamination crack tip. A compliance-based fracture mechanics approach is used again to express the mode II energy release rate in terms of the applied loading and the test specimen geometry. The elastic compliance was first derived (refs. 41 and 42) from beam theory. For a unidirectionally reinforced laminate, the compliance is

$$C(a) = \frac{\delta}{P} = \frac{2L^3 + 3a^3}{8EBh^3} \qquad (14)$$

where δ is the load-point displacement, $E = E_{11}$ is the modulus in the fiber direction, and load P is applied at the midspan (fig. 18). Following the procedure previously outlined, the energy release rate, from equation (5), is

$$G_{II} = \frac{9P^2a^2}{16EB^2h^3} \qquad (15)$$

where the energy release rate in this case is designated G_{II} because the crack is under mode II loading. A finite element analysis was used in reference 43 to show that this beam model of the ENF specimen, eq. (15), predicted G_{II} with less than 10 percent error for crack lengths for which $a/L \geq 0.5$.

Shear compliance. – The effects of shear deformation on the ENF specimen compliance are significant for specimens

with large aspect ratios (h/L) and for highly orthotropic materials. When shear compliance is included, the overall compliance (ref. 44) of the test specimen is

$$C(a) = \frac{2L^3 + 3a^3}{8EBh^3}\ (1 + S) \qquad (16)$$

where S is the compliance due to shear deformation, given by

$$S = 2h^2\ \frac{E_{11}}{G_{13}}\ \frac{1.2L + 0.9a}{2L^3 + 3a^3}$$

and G_{13} is the transverse shear modulus. From equation (5), the energy release rate is therefore

$$G_{II} = \frac{9P^2a^2}{16EB^2h^3}\left[1 + 0.2\ \frac{E_{11}}{G_{13}}\left(\frac{h}{a}\right)^2\right] \qquad (17)$$

when shear deformation is accounted for.

Friction effects. – When a transverse load is applied to the ENF test specimen, the crack surfaces come into contact. Friction between crack surfaces can retard crack growth by dissipating energy that would otherwise be used as fracture energy. As the delamination extends and more fracture surface area is generated, this effect may become more pronounced. The reduced energy available for fracture is derived in reference 44 as

$$G_{II}(\mu) = G_{II} - \frac{3P^2\mu a}{4EB^2h^2} \qquad (18)$$

where the last term is the energy dissipated through friction, and μ is the coefficient of friction between the contacting crack surfaces. Although the actual coefficient of friction is difficult to obtain, reference 43 shows that frictional effects on the energy release rate are negligible for aspect ratios a/L greater than 0.5 if $\mu \le 0.3$.

Data Reduction Procedures: ENF Specimen

A typical load-displacement curve for an ENF test specimen made from a brittle matrix composite is shown in figure 19. Several approaches are described here that can be used to determine G_{IIc} from this type of test.

Compliance calibration method. – This approach is similar to the beam analysis method given for the DCB specimen and is described more thoroughly in reference 45. The compliance of the ENF specimen (eq. (14)), can be re-written as

$$C(a) = \left(\frac{3}{8EBh^3}\right)\ a^3 + \frac{2L^3}{8EBh^3}$$

$$= ma^3 + \text{constant} \qquad (19)$$

The parameter m is determined from a curve fit of the compliance versus crack length, as shown in figure 20. Equations (14) and (15) can be combined to give

$$G_{II} = \frac{9P^2a^2}{2B\left(2L^3 + 3a^3\right)}\ C(a) \qquad (20)$$

Therefore the mode II fracture toughness is

$$G_{IIc} = \left(\frac{3P_c^2a^2}{2B}\right)\ m \qquad (21)$$

Where P_c is the critical load that causes a delamination of length a to propagate and m is the effective measured value of the term in parentheses in equation (19), estimated from the slope of the plot in figure 20. An experimental error in measurement of the delamination crack length will therefore result in more data scatter in G_{IIc} than for G_{Ic}, (eq. (10)) because of the a^2 term in the numerator of equation (21).

Modified compliance calibration method. – A compliance calibration method incorporating the effects of shear compliance is described in reference 47. Equation (16) can be written as

$$C(a) = \frac{2L^3}{8EBh^3}\left[1 + 1.2\gamma + 0.9\gamma\frac{a}{L} + 1.5\left(\frac{a}{L}\right)^3\right] \qquad (22)$$

where $E = E_{11}$, and

$$\gamma = \left(\frac{h}{L}\right)^2\ \frac{E_{11}}{G_{13}}$$

The compliance for an uncracked specimen (a=0) is therefore:

$$C_0 = \frac{2L^3}{8EBh^3}\ (1 + 1.2\gamma) \qquad (23)$$

Dividing equation (22) by equation (23) gives

$$\frac{C}{C_0} = A_0 + A_1\left(\frac{a}{L}\right) + A_3\left(\frac{a}{L}\right)^3 \qquad (24)$$

The coefficients A_0, A_1, and A_3 are determined from a least-squares fit of the compliance versus crack length curve, normalized by the (constant) C_0 of the uncracked ENF specimen. From equation (5), the energy release rate is

$$G_{II} = \frac{P^2C_0}{2BL}\left[A_1 + 3A_3\left(\frac{a}{L}\right)^2\right] \qquad (25)$$

The fracture toughness G_{IIc} is calculated by using equation (25) at the critical load $P = P_c$ just prior to crack extension.

Beam analysis method. – Results of finite element analysis presented in reference 48 indicate that beam theory models will accurately predict the overall compliance of the ENF specimen if transverse shear effects are included. However, because they cannot account for the high shear stress near the crack tip, the beam theory models may underestimate G_{II} by 20 to 40 percent, depending on the dimensions and material orthotropy of the test specimen. Two non-dimensional correction factors γ and β were derived to curve-fit the beam theory estimates of G_{II} to the finite element results:

$$\frac{G_{II}^{FE}}{G_{II}^{BT}} = \alpha + \beta\ \frac{E_{11}}{G_{13}}\left(\frac{h}{a}\right)^2$$

The curve-fit parameters α and β are given in reference 48 for several typical test specimen dimensions. The beam theory

estimate of G_{II} is determined from the measured compliance by using equation (20).

Area method. – A loading curve typical for an ENF test of a toughened-matrix composite is shown in figure 21. Because of the nonlinear elastic deformation of the matrix, the area method should be used to determine G_{IIc}. This approach was described earlier for data reduction of the DCB specimen.

Design Considerations: ENF Specimen

This section gives the guidelines for the effective design of ENF test specimens. Variables that are considered include ply thickness, initial crack length, and specimen aspect ratio (a/L). In the cases considered here, a 0° unidirectional layup is assumed.

Initial crack length. – If the data analysis method does not account for shear deformation, the dimensions of the test specimen should be chosen so as to minimize the shear contribution. As shown in figure 22 and equation (17), the effect of shear compliance decreases with crack length. For highly orthotropic materials such as graphite-epoxy ($E_{11}/G_{13} \simeq 30$), shear compliance adds less than 2 percent to the apparent fracture resistance of the material for $(a/h) \geq 18$. This would correspond to a crack length of approximately 2.5 cm for a 20-ply graphite-epoxy laminate.

Specimen thickness. – Linear elastic material behavior and small deflection theory are assumed in the beam theory model of the ENF test specimen. The specimen dimensions must be chosen so that these assumptions will be valid. Based on the material linearity criterion, a minimum thickness requirement is derived in reference 44 as

$$h \geq \frac{L^2 G_{IIc}}{a^2 \varepsilon^2 E_{11}}$$

where ε is the maximum allowable strain at which the deformation is linear elastic.

Based on the small deflection criterion, a second thickness requirement is derived in reference 44:

$$h^3 \geq \frac{G_{IIc}\left(L^2 + 3a^2\right)^2}{4E_{11}a^2(y')^2}$$

where y' is the maximum allowable slope, chosen so as to minimize the error induced by using the small deflection beam theory.

These two thickness requirements should be used to determine the minimum number of plies needed by the ENF specimen to assure a valid G_{IIc} measurement. The small deflection requirement determines the minimum thickness for brittle materials, but the material linearity requirement determines the thickness for tougher materials (fig. 23).

Specimen length. – In ENF tests, the specimen length is generally chosen so that $a/L = 0.5$, thereby ensuring that the crack tip is initially halfway between the loading point and the support pin (fig. 18). This arrangement can be expected to minimize the frictional effects at the crack tip and was shown (ref. 41) to induce an error of less than 2 percent in the measured value of G_{IIc} because of crack surface friction for AS1/3501-6 composites.

An analysis of the crack stability (ref. 44), however, showed that crack growth is unstable under fixed-grip conditions for $a/L < 0.7$, indicating that the specimen length should be chosen so that $a/L \geq 0.7$, to produce stable crack growth.

Precracking. – The initial crack is usually introduced into the laminate by placing a thin ($\simeq$ 1 mil) nonadhesive insert between the two midplane plies before curing (fig. 3). The crack tip at the end of the insert is blunt, however, and therefore results in higher measurements of G_{IIc} (refs. 42, 46, and 47) than would be obtained from mode II delaminations occurring naturally from high interlaminar shear stresses. To produce a sharper crack tip, the ENF specimen is given either a static three-point bending load (ref. 42) or a low-amplitude cyclic load (ref. 47) sufficient to cause a small extension of the original embedded delamination. The natural crack extension caused by this "precracking" procedure has a sharper crack tip and therefore usually results in lower and more consistent measurements of G_{IIc}.

End-Loaded Split Test

A second, less frequently used test for pure mode II loading is the end-loaded split (ELS) specimen, which is similar to the DCB specimen but has different loading and boundary conditions (fig. 24). In reference 49 the elastic compliance was derived as

$$C(a) = \frac{L^3 + 3a^3}{2E_{11}Bh^3} \tag{26}$$

the mode II energy release rate from equation (5) is therefore

$$G_{II} = \frac{9P^2a^2}{4E_{11}B^2h^3} \tag{27}$$

Data Reduction Procedures

The compliance and energy release rate are similar to those of the ENF specimen, so similar data reduction procedures are used for calculating G_{IIc} from the test data.

Beam analysis method. – The mode II energy release rate in equation (27) can be written as

$$G_{II} = \frac{9P^2a^2}{2B\left(L^3 + 3a^3\right)} \quad C(a)$$

where $C(a) = \delta/P$ is the measured compliance. The fracture toughness is determined by calculating G_{II} at the critical load P_c that causes crack extension.

Compliance calibration method. – The compliance of the ELS specimen, given in equation (26), can be written as

$$C(a) = \frac{3}{2EBh^3} a^3 + \frac{L^3}{2EBh^3}$$

$$= ma^3 + \text{constant} \qquad (28)$$

The parameter m can be measured from a curve-fit of the compliance versus a^3 graph as shown in figure 20 for the ENF specimen. Equations (5) and (28) can be combined to give the mode II fracture toughness:

$$G_{IIc} = \left(\frac{3P_c^2a^2}{2B}\right) m$$

where P_c is the critical load that causes a delamination of length 'a' to propagate. Tests show (ref. 40) that there is more scatter in G_{IIc} measurements when the ELS specimen is used than when the ENF specimen is used, because the crack length is harder to measure accurately.

Mode II toughness measurements for a variety of different composites are given in table II in appendix B.

Mixed-Mode Loading

Delamination can originate in mode I because of transverse tensile stress, σ_{yy}; in mode II because of in-plane shear stress, σ_{xy}; or in mode III because of out-of-plane shear stress, σ_{xy}. Therefore, a general, combined stress state at the ply interface will produce a combination of modes I, II, and III. In actual structural applications, composite materials are subjected to a combined stress state. It is therefore necessary to evaluate the fracture resistance of composites under mixed-mode loading and to develop an appropriate criterion that describes the "failure envelope" for a given material under mixed-mode loading.

This section is divided into two parts. First, the cracked-lap shear and the edge delamination tension tests that produce mixed mode I-mode II loading conditions are discussed. Second, an overview of mixed-mode failure criteria used to quantify interlaminar fracture resistance under combined mode I-mode II loading is presented.

Cracked-Lap Shear Test

The cracked-lap shear (CLS) specimen was originally developed for testing adhesive bonds between metals (ref. 7) and was first used to evaluate mixed-mode fracture toughness of composites in reference 50. Progressive debonding of composite adhesive joints during fatigue loading was evaluated with CLS specimens in references 32, 37, and 51.

A typical composite CLS specimen is shown in figure 25. The mode I component of the loading is due to the bending moment induced at the crack tip by the eccentric load path. The compliance of the CLS specimen is given (ref. 50) by

$$C(a) = \frac{1}{EBh_2}\left[2L + a\left(\frac{h_1}{h_2} - 1\right)\right] \qquad (29)$$

where h_1 and h_2 are the thickness of the test specimen's two sections (fig. 25); $E = (E_{11})$ is the stiffness in the fiber direction. The other variables have the same definitions as used previously. From equation (5), the total energy release rate is given as

$$G_{total} = G_I + G_{II} = \frac{P^2}{2EB^2}\left(\frac{h_1 - h_2}{h_1h_2}\right) \qquad (30)$$

The critical total energy release rate at the onset of crack extension is therefore determined by calculating G_{total} from equation (30) at the critical load P_c, just before crack extension occurs. Additional analysis is required to determine the relative amounts that G_I and G_{II} contribute to the total energy release rate. One means of accomplishing this is with finite element analysis. Due to the out-of-plane displacements and rotations that result from the eccentric load path, a geometrically nonlinear finite element analysis is required to determine the proportions of mode I and mode II loading at the delamination crack tip (ref. 52). A local crack-closure method (ref. 53) was used to calculate the energy released during crack extension; a unidirectional graphite/epoxy CLS specimen with a midplane delamination ($h_1 = 2h_2$) was shown (ref. 50) to have 23.5 percent mode I loading, that is

$$\frac{G_I}{G_{total}} = 0.235$$

It was also shown that this ratio is independent of crack length. An explicit solution for G_I in terms of the bending moment at the crack tip is given in reference 7. These calculations are supported by the test results that showed the loading to be approximately 20 percent mode I (ref. 42) for unidirectionally reinforced CLS specimens with midplane delaminations. The ratio of G_I to G_{II} can be varied by changing the relative thickness (h_1 and h_2) of the two sections (refs. 7 and 52).

Data Reduction Procedures: CLS Specimen

Two approaches used to calculate the mixed-mode fracture toughness from CLS test data are described below.

Compliance calibration method. – Equations (29) and (30) indicate that the CLS specimen compliance varies linearly with crack length, and that the critical load P_c that causes delamination is independent of crack length. This was verified by test measurements (refs. 37 and 50) and finite element analysis (ref. 52). The slope calculated from a linear curve fit of the compliance versus crack length curve can be used with equation (5) to calculate the total critical energy release rate

$$G_c^{total} = \frac{P_c^2}{2B}\frac{dC}{da}$$

The derivative is taken as the slope of the line in figure 26, and the critical load P_c is determined from the same load versus displacement data as shown in figure 27.

Strain gauge method. – Strain gauge measurements from a CLS specimen can be used to determine mixed-mode fracture toughness (ref. 42) in the following manner. The load P

produces axial strains ε_1 and ε_2 in the two sections of the specimen so that

$$P = E_1 A_1 \varepsilon_1 = E_2 A_2 \varepsilon_2$$

where ε_1, ε_2 are the longitudinal (fiber direction) moduli for sections 1 and 2, and A_1, A_2 are the cross sectional areas of the two sections. Therefore, i=1 and 2,

$$\varepsilon_i A_i = \frac{dP}{d\varepsilon_i}$$

so equation (30) can be written

$$G_I + G_{II} = \frac{P^2}{2B}\left(\frac{d\varepsilon_2}{dP} - \frac{d\varepsilon_1}{dP}\right)$$

where the derivatives are determined from plots of strain versus load for each section.

Design Considerations: CLS Specimen

The CLS specimen can fail either in tension or by delamination. The specimen must therefore be designed so that the tensile failure load is higher than the load required to cause delamination. Following reference 54, we have, from equation (30),

$$P_c = B\sqrt{2Eh^* G_c} \qquad (31)$$

where P_c is the critical load required to cause delamination and

$$h^* = \frac{h_1 h_2}{h_1 - h_2}$$

To ensure that the load required for delamination is lower than that for tensile failure, the condition

$$P_c B h_2 < S_{11} \qquad (32)$$

must be satisfied, where S_{11} is the longitudinal tensile strength of the laminate. Substituting equation (31) into equation (32) gives the design requirement that the CLS specimen thickness be determined by

$$h_2\left(1 - \frac{h_2}{h_1}\right) > \frac{2EG_c}{(S_{11})^2}$$

to avoid tensile failure.

Edge-Delamination Tension Test

Edge delaminations are likely to begin in a composite laminate under uniaxial tension due to the high interlaminar stresses near the free edge (refs. 55 and 56). In reference 57, free-edge delamination specimens were designed by choosing the laminate ply orientations so that the Poisson's ratio mismatch between plies was maximized, thereby making them susceptible to free-edge delaminati on. An approximate stress analysis of a $[\pm\theta_1,\theta_2]_{sym}$ HTS/ERLA 2256 graphite/epoxy laminate under uniaxial tension was used to show that values of $\theta_1 = 25°$ and $\theta_2 = 90°$ would maximize the interlaminar normal stress at the midplane near the free edge of the laminate, thus initiating a pure mode I edge delamination. A mixed-mode delamination could begin at the -25°/90° interface (ref. 58), however, depending on the values of mode I and mixed-mode fracture toughness.

A similar approach was used in designing the edge-delamination tension (EDT) specimen (refs. 59 to 61) to estimate the mixed-mode fracture toughness for a T300/5208 composite. Interlaminar tensile stresses in an 11-ply $[(\pm 30°)_2, 90°, \underline{90°}]_{sym}$ laminate cause free-edge delaminations to initiate under uniaxial tension at the -30°/90° interfaces (fig. 28). As the load is progressively increased and the delaminations grow inward from the edges, radiographic examinations are used to measure the delaminated area. The measured delaminations are approximated by rectangles of equivalent area (fig. 29), so the stiffness after delamination can be estimated by

$$E = E_{lam} + (E^* - E_{lam})\frac{a}{b} \qquad (33)$$

where the rectangular delaminations have uniform length a and the width of the laminate is 2b. The delaminations are assumed to grow symmetrically at both -30°/90° interfaces. The delaminated ply groups in figure 28 are also assumed to act independently in supporting the applied load, so that

$$E^* = \frac{8E_{\pm 30} + 3E_{90}}{11}$$

is the laminate stiffness in the loading direction for the fully delaminated case (a = b); E_{lam} is the stiffness before delamination; and the [±30°] and [90°] sublaminates stiffnesses are determined either from classical lamination theory or from separate tests.

The energy release rate is determined by using Hooke's law in equation (10) and assuming that the work term vanishes because of fixed grip conditions. The total energy release rate is then approximated by

$$G_I + G_{II} = -V\frac{\varepsilon^2}{2}\frac{dE}{dA}$$

where V = 2blt is the volume of the test specimen, ε is the nominal strain in the loading direction, and the derivative obtained by differentiating equation (33), represents the stiffness loss per unit crack area. This gives

$$G_I + G_{II} = \frac{\varepsilon^2 t}{2}(E_{lam} - E^*) \qquad (34)$$

so the mixed-mode fracture toughness is determined from equation (34) and the critical strain level ε_c at which crack initiation occurs. The critical strain ε_c is indicated by the onset of nonlinear load-displacement behavior (ref. 61). Equation (34) indicates that the energy release rate is independent of crack length. Finite element analysis (ref. 61) showed that the delamination is 57 percent mode I; that is,

$$\frac{G_I}{G_I + G_{II}} = 0.57$$

for the EDT specimen with this particular material and layup. However, mode I percentages ranging from 22 to 90 percent

have been achieved for T300/5208 EDT specimens (ref. 62) by varying the ply layup.

Examination of failed EDT specimens shows that the multiple delaminations do not grow symmetrically, nor do they grow in a self-similar manner. Considerable intraply cracking occurs in the 90° plies as the cracks wander between the two -30°/90° interfaces. A modified free-edge delamination test was devised (ref. 63) to remedy these problems. In this case, nonadhesive inserts were used to initiate pure mode I delaminations along the midplane at the free edges of a $[\pm 30°/\mp 30°/90°_2]_{sym}$ graphite/epoxy laminate. The inserts promote self-similar crack growth between the two 90° plies and therefore eliminate any crack wandering that may otherwise occur. Thermal residual stresses also increase the calculated mode I fracture toughness (refs. 63 and 64) by approximately 15 percent, and should therefore be accounted for in the data reduction process. However, for reasons that are unclear, measured values of G_{Ic} are considerably lower than those from DCB tests. Mixed-mode toughness measurments for a variety of different composites are given in table III of appendix B.

Mixed-Mode Fracture Criteria

In this section, several different criteria are summarized to predict the onset of delamination under mixed-mode loading. One assumption is that crack growth occurs when the total energy release rate reaches a critical value:

$$G_I + G_{II} = G_c$$

This criterion was used to predict the progressive interlaminar fracture at three different ply interfaces of a unidirectional glass/epoxy material (refs. 65 and 66) under a monotonically increasing tensile load (fig. 30). The fracture was predicted by incorporating the failure criterion into a finite element program and using singular elements to model the stresses near the crack tip.

A general, mixed-mode failure criterion should account for the different interlaminar fracture toughnesses observed with different fracture modes. For brittle-matrix composites, G_{IIc} can be as much as 10 times greater than G_{Ic} (refs. 28 and 39). This difference is accounted for by explicitly including the values of G_{Ic} and G_{IIc} in the failure criterion. The modified form

$$\left[\frac{G_I}{G_{Ic}}\right]^n + \left[\frac{G_{II}}{G_{IIc}}\right]^n = 1 \qquad (35)$$

was therefore proposed (refs. 32 and 42) as a general criterion for interlaminar fracture under an arbitrary mixed-mode loading.

In reference 39, test data for three different epoxy-matrix composites over a range of mixed-mode loading ratios were used to determine an appropriate value for the exponent in equation (35). The data in figure 31 were taken from mixed-mode fracture tests of three different types of composites. Because the matrix materials have widely different ductilities, the test results illustrate the wide range of fracture toughness that different epoxy-matrix composites can display.

Fracture-toughness measurements are shown in figure 31(a) for a brittle (Narmco 5208) epoxy-matrix composite, in figure 31(b) for a more ductile (Hexcel Hx205) epoxy-matrix composite with an extended polymer chain, and in figure 31(c) for a composite with an extended chain epoxy matrix (Hexcel F-185), modified with rubber additives for increased ductility and toughness. In all cases, a linear curve fit can be used to approximate the test data (fig. 32). This would suggest that an exponent of $n = 1$ can be used in the mixed-mode failure criterion, equation (35), regardless of material. This same failure criterion (with exponent $n = 1$) also accurately predicted (refs. 42 and 67) the initiation of delamination crack extension in AS1/3501-6 fracture specimens under a variety of mixed-mode loading ratios.

The results of a separate series of fracture tests (ref. 28) on a wide variety of material systems are shown in figure 33. In this case, the "failure envelopes" cannot all be represented by linear approximations, which indicates that the exponent n in equation (35) may in fact be a variable, dependent on the particular fiber/matrix system.

Rate-Dependent Behavior

Most of the research on rate-dependent fracture in composites has been done using mode I loading with the DCB test. The results presented and discussed in this section therefore reflect this. The variation of fracture toughness with loading rate is most appropriately expressed in terms of crack propagation velocity; however, the most frequently used measure of loading rate is the speed at which the opening displacement is imposed on the DCB test specimen. This is determined from the cross-head displacement rate on the test machine. Therefore, the opening displacement rate is used here as a common measure of loading rate to compare the results of different tests.

Brittle-Matrix Composites

Most research in rate-dependent fracture behavior of composites has been on brittle-matrix materials. The earliest work in this area is reported in reference 10. E-glass/epoxy DCB specimens were tested over a range of opening displacement rates ($5\times10^{-3} \le \dot{\delta} \le 5$ mm/sec). G_{Ic} almost doubled over this range of loading rates and crack propagation speeds ($\dot{a}$) of up to 1 mm/sec were reached. Calculation of crack propagation speed from the cross-head displacement rate produced data that fit the trend

$$G_{Ic} = K\dot{a}^n \qquad (36)$$

where K and n are constants, $K = 1288$ J/m^2 and $n = 0.1$ (fig. 34). Results presented in reference 11 for AS4/3501–6 graphite/epoxy over a similar range of loading rates show no significant G_{Ic} variation from the static fracture toughness. However, fracture toughness increases at higher loading rates for the same material. A 28-percent increase in G_{Ic} was measured for AS4/3501–6 composites (ref. 68) for opening

displacement rates in the range $0.009 \leq \dot{\delta} \leq 8.5$ mm/sec, which produced crack propagation velocities of up to 51 mm/sec. The data follow a trend similar to that shown in figure 34 and equation (36), and the parameters $K = 210$ J/m^2 and $n = 0.035$ are determined from the curve fit. Similarly, a 25-percent increase in G_{Ic} was measured in tests of C6000/PMR–15 composites (ref. 22) over approximately the same range of loading rates.

Crack propagation speeds up to 26 m/sec were obtained (ref. 19) in AS4/3501–6 composites with a DCB specimen tapered in the height direction. This tapering eliminated the intermittent crack-arrest ("slip-stick") phenomenon by slightly decreasing compliance with crack length. The test data (fig. 35) were represented by a third-order curve fit of the form

$$\log G_{Ic} = \sum_{n=0}^{N} A_n (\log \dot{a})^n$$

The fracture toughness of brittle-matrix composites increases with crack propagation velocity until it reaches a maximum value at $\dot{a} \simeq 1$ m/sec, and it decreases thereafter. The maximum G_{Ic} is approximately 46 percent higher than the fracture toughness measured under static loading conditions.

At very high loading rates, the fracture toughness of 90° AS/3501–6 laminates (ref. 69) increased exponentially with crack speed (ref. 70):

$$G_{Ic} = C_1 \exp(C_2 \dot{a})$$

as shown in figure 36.

Toughened-Matrix Composites

Relatively little research has been done on loading rate effects on fracture in toughened-matrix composites, but the available data suggest that the mode I fracture toughness of the composite is determined to a large extent by the viscoelastic nature of the matrix.

Viscoelastic behavior of a neat elastomer-toughened epoxy causes the variation of mode I fracture energy with temperature and loading rate shown in figure 37. At high loading rates, the matrix behaves in a brittle manner, and the fracture energy decreases to that of the unmodified, brittle epoxy because the crack tip deformation zone has less time to develop (ref. 11), so the material cannot redistribute the high crack tip stresses prior to fracture.

Composites with a toughened matrix also exhibit rate-dependent fracture behavior, although not to the extent observed in the neat matrix because of the constraint on matrix deformation imposed by the fibers. Hexcel F-185 is an epoxy resin with carboxy-terminated butadiene acrylonitride (CTBN) rubber additives to increase ductility and toughness. In reference 8, the mode I fracture toughness of a T300/F-185 composite was measured at different loading rates by varying the displacement rate in DCB specimens over the range $0.0085 \leq \dot{\delta} \leq 8.5$ mm/sec. Maximum crack propagation velocities were estimated from strain gauge measurements to be 21 mm/sec. The mode I fracture toughness decreased by 20 percent over this range of crack velocities, probably because the progressively decreasing size of the crack tip deformation zone (fig. 38) caused the composite to exhibit a more brittle fracture behavior at higher loading rates. The data followed a trend described by equation (36), and the values $n = 0.027$ and $K = 1.63$ kJ/m^2 were determined from a curve-fit of the test data shown in figure 39.

At lower loading rates, no rate sensitivity in G_{Ic} is apparent. Three different graphite fabric-epoxy matrix composites with varying amounts of elastomer additives were tested over a range of loading rates (ref. 72) by varying the displacement rate in DCB tests within the range $5 \times 10^{-4} < \dot{\delta} < 1$ mm/sec. Test results showed no significant variation in G_{Ic}.

Mode II Loading

Because of the difficulty in measuring crack length and load under dynamic conditions in mode II, dynamic fracture-toughness measurements are particularly difficult to make. A combined experimental-numerical approach was used (refs. 73 and 74) to estimate G_{IIc} for T300/934 graphite-epoxy composites. Finite element analysis (ref. 73) was used to verify that a symmetric, cantilevered laminate with a through-the-width delamination embedded along the midplane (fig. 40) would produce nearly pure-mode-II deformation at the crack tip under transverse impact loading.

A series of identical $[0°/90°]_{5S}$ cross-ply test specimens were impacted over a range of velocities, and the post-impact crack lengths were measured with ultrasonic C-scans. The critical level of impact energy required to cause a small extension of an initial embedded delamination was determined from a plot of post-impact delamination length (fig. 40). A finite element analysis of the test specimen impacted at the critical energy (ref. 74) was then used to calculate the time-dependent energy release rate (fig. 41). Since the analysis corresponds to the critical case in which the impact energy is exactly that required to cause a small extension of the initial crack, the maximum energy release rate should be equal to the fracture toughness, G_{IIc}, for the material. This was verified (ref. 74) by showing that G_{IIc} determined in this manner was a material property, independent of crack length.

Design of Tough Composites

Various approaches have been used to design composite laminates for high interlaminar fracture resistance. Several of the most frequently used methods will be discussed here.

Matrix Properties

The fracture toughness of the neat resin is the most significant variable affecting the interlaminar fracture toughness of the composite. The primary factors that determine the fracture toughness of a polymer are its ductility and the extent of cross-linking in the polymer chain (refs. 1, 34 and 75). Matrix

toughness increases with ductility and decreases with the amount of cross-linking. For example, Hercules 3502 is a highly cross-linked, brittle epoxy with mode I fracture toughness $G_{Ic} \simeq 70$ J/m^2 (appendix B, table I), whereas Hexcel Hx205 has lower cross-link density (ref. 76) and a fracture toughness of 230 to 340 J/m^2. Resin ductility also increases fracture toughness. The composition of F-185 epoxy is the same as that of Hx205 except for the addition of 13.7 percent CTBN rubber particles to increase ductility (refs. 17 and 39). The mode I fracture toughness of toughened F-185 epoxy has been measured at 5 to 8 kJ/m^2 (appendix B, table I). Detailed information about the particle sizes and matrix properties required to achieve optimum toughening by adding rubber particles to the neat resin is given in references 34, 39 and 77. References 39 and 51 show that toughening an epoxy with rubber additives does not increase G_{IIc} nearly as much as G_{Ic}. This is evident from the trend observed in figure 31 for the three material systems with progressively increasing toughness; it is the result of the lack of matrix dilatation that is required near the crack tip under mode II loading (refs. 28 and 39).

Composite interlaminar fracture toughness varies in a complex way with neat resin toughness. For brittle polymers ($G_{Ic} \leq 200$ J/m^2), the fracture toughness of the composite is usually two to three times greater than that of the neat resin. This difference has been attributed (ref. 30) to the additional energy-absorbing mechanisms of fiber pullout and fiber breakage that can occur in the composite. For tougher polymers ($G_{Ic} > 200$ J/m^2), however, the size of the crack tip plastic zone in the composite is limited by the constraining effect of the surrounding fibers (refs. 28, 30 and 77) as shown in figure 42. The constraining effect limits the ability of the matrix to redistribute the high stresses near the crack tip and causes the composite to fracture in a more brittle manner than the neat matrix. In figure 43, mode I interlaminar fracture toughnesses of a variety of different composites are plotted as a function of neat resin toughness. The trend is bilinear, changing slope near 200 J/m^2, which is approximately the point at which the crack tip plastic zone in the matrix is equal to the average fiber spacing (refs. 28 and 30) in the composite.

Therefore, large increases in neat resin toughness are not fully transferred to the composite because of the constraint imposed by the fibers on the size of the crack tip plastic zone. For example, the data from reference 36 in appendix B, table I indicate that the addition of 9 percent CTBN elastomer to the neat MY750 epoxy increased the matrix toughness by a factor of 10 but the composite toughness only by a factor of 2.

Interply Layer

Interply layers are a means of toughening the composite without the large decrease in compression strength in hot and wet environments that usually occurs when the composite is toughened with matrix additives (ref. 76). Delaminations occur at ply interfaces because the thin, resin-rich layer between plies cannot undergo shear deformation. Toughening can therefore be achieved by adding a discrete layer of a second, tougher resin between plies of the laminate, where high interlaminar shear stresses occur. This toughening approach, first used in the CYCOM HST–7 system (refs. 78 and 79), was shown (ref. 80) to double G_{IIc} in some graphite/epoxy systems, while 20- to 50-percent increases in G_{Ic} were measured (ref. 81). In comparison, a sixfold increase in G_{Ic} and a fourfold increase in G_{IIc} were obtained for AS4/3502 graphite/epoxy (ref. 82) with an FM-300 adhesive interply layer. An order-of-magnitude increase in G_{Ic} was measured (ref. 83) with a toughened AF–163 adhesive interply layer along the midplane of AS1/3502 DCB specimens. The interply layer also reduced the amount of delamination due to transverse impact loading. Impact damage usually initiates as transverse matrix cracks, which cause delaminations to form when they reach a ply interface. Tough interply layers were shown (refs. 78 and 79) to arrest impact-induced matrix cracks, thereby preventing delaminations from forming along the ply interfaces and increasing the compression strength after impact.

Similarly, tough adhesive strips of finite width can be embedded selectively at delamination-prone locations to arrest propagating delaminations. Finite-width strips of American Cyanamid FM–1000 adhesive, placed as indicated in figure 44, were shown (ref. 84) to arrest edge delaminations in AS4/3501–6 laminates, thereby resulting in an increase in static tensile strength and an extension of fatigue life (fig. 45).

Fiber-Matrix Bond

An increase in interlaminar fracture toughness in brittle composites, can be obtained by increasing the strength of the bond between fiber and matrix. In reference 85, a scanning electron microscope was used to observe in situ delamination. The results indicated that mode I delaminations in brittle-matrix composites grew primarily by the progressive failure of the fiber/matrix interface region. In tougher composites, crack propagation occurred primarily by fracture through the matrix, with little interfacial failure. In the latter case, a better interfacial bond resulted in the toughness of the resin being more fully utilized in the composite. A similar dependence of interlaminar fracture toughness with fiber-matrix bond strength was reported (ref. 41) for mode II loading.

The fiber/matrix bond strength and/or toughness can be increased by applying a polymer coating to the fiber surface (refs. 86 and 87). A 50-percent increase in G_{Ic} was reported (ref. 88) for AS4/MDA (methylene dianiline epoxy) composites when a thin, tough copolymer layer was applied to the fibers with an electropolymerization process (ref. 89), as shown in figure 46. However, this was accompanied by a large decrease in G_{IIc}, which was attributed to the failure of the matrix/interface bond. Applying coatings of toughened-epoxy adhesives (an elastomer-modified epoxy, AF–163–2 from 3M) to AS4 graphite fibers (ref. 90) increased the mode I fracture toughness of AS4/976 composites from their baseline value of 88 J/m^2 to 300 to 500 J/m^2, depending on the fiber volume fraction of the laminate. However, the fiber-coating method of toughening may adversely affect the matrix-dominated

properties of laminate. If a significant amount of low-modulus resin is added to the laminate, the compression strength can be decreased.

Layup

Ply orientations and fiber architecture can affect delamination resistance through several different physical mechanisms. In reference 57, fabrication-induced residual stresses were shown to play an important role. An approximate analysis of interlaminar stresses near the free edge of a laminate was used to design two types of laminates. A $[(\pm 25)_2^\circ/90^\circ]_{sym}$ laminate has maximum tensile residual stress at the midplane near the free edge and is therefore prone to delaminate under uniaxial tension at that location. In contrast, a $[90^\circ/(\pm 25)_2^\circ]_{sym}$ laminate has compressive residual stresses at all interfaces and is more delamination resistant. Tests showed that edge delaminations initiated in the former laminate at approximately 50 percent of the ultimate failure load, whereas no delamination was visible prior to tensile failure in the latter specimen.

The data from reference 31 in appendix B, table I indicate no significant difference in G_{Ic} measured at 0°/0°, 0°/45°, and ±45° interfaces in DCB specimens of brittle T300/5208 or tougher T300/BP907 graphite-epoxy materials. This suggests that fracture toughness is independent of delamination interface. However, a woven glass or graphite fiber reinforcement (ref. 17) increases resistance to delamination by a factor of 2 to 3 compared to unidirectional reinforcement. The additional fracture resistance is probably due to the irregular path the delamination must take to separate the plies.

The ply orientations in a laminate also affect the ability of fibers in neighboring plies to nest together (refs. 23 and 34), which in turn affects the thickness of the resin-rich interply layer in the cured laminate by changing the amount of resin that bleeds away from the interlaminar region during the cure cycle. The thickness of the interply layer can therefore be controlled somewhat by varying the number of 90° "bleeder plies" (ref. 24) in the laminate. Using this approach for AS/3501–6 laminates caused G_{IIc} to increase linearly with thickness of the interply layer over the range $5 \leq t_m \leq 15$ μm, while the interlaminar shear strength was unaffected by the increase in interply layer thickness. A difference in G_{IIc} of $\simeq$ 50 percent was measured, depending on the interply layer thickness, as shown in figure 47. The mode I fracture toughness decreases with an increase in interply thickness, however, because of the reduced fiber volume fraction within the interply layer, which decreases the amount of fiber bridging (ref. 23) occurring under mode I loading.

Conclusion

A review of the test results shows that a standard specimen geometry is needed to obtain consistent fracture toughness measurements in composites. In general, the measured toughness values vary more as the toughness of the material increases. This variability could be caused by incorrect sizing of the test specimen and/or the inappropriate assumption of linear elastic deformation. A standard data reduction procedure may therefore be needed as well, particularly for the tougher materials. A standard test for Mode I, interlaminar fracture (G_{Ic}), which uses the DCB specimen, is being developed by The American Society for Testing and Materials (ASTM) Committee D30 on composite materials.

Relatively little work has been reported on the effect on fracture toughness of fiber orientation, fiber architecture (continuous versus chopped or woven-fiber reinforcements), or fiber surface treatment. However, the available data indicate that both woven-fiber reinforcement and fiber-surface treatments significantly increase toughness. This should make these approaches useful to structural engineers and designers. Since the mechanisms by which they increase fracture toughness are not well understood, these approaches are still of considerable research interest.

Lewis Research Center
National Aeronautics and Space Administration
Cleveland, Ohio August 12, 1992

References

1. Williams, J.G.: Fracture Mechanics of Polymers. Halsted Press, 1984.
2. Broek, D.: Elementary Engineering of Fracture Mechanics. Martinus Nijhoff, 1982.
3. Ripling, E.J.; Mostovoy, S.; and Patrick, R.L.: Application of Fracture Mechanics to Adhesive Joints. Adhesion, ASTM–STP–360, 1964, pp. 5–19.
4. Whitney, J.M.; Browning, C.E.; and Hoogsteden, W.: A Double Cantilever Beam Test for Characterizing Mode I Delamination of Composite Materials. J. Reinf. Compos. Mater., vol. 1, no. 4, 1982, pp. 297–313.
5. Wilkins, D.J.; et al.: Characterizing Delamination Growth in Graphite-Epoxy. Damage in Composite Materials, K.L. Reifsnider, ed., ASTM–STP–775, 1982, pp. 168–183.
6. Whitney, J.M.; Browning, C.E.; and Mair, A.: Analysis of the Flexure Test for Laminated Composite Materials. Composite Materials: Testing and Design (Third Conference), ASTM–STP–546, 1973, pp. 30–45.
7. Brussat, T.R.; Chiu, S.T.; and Mostovoy, S.: Fracture Mechanics for Structural Adhesive Bonds. AFML–TR–77–163, Oct. 1977. (Avail. NTIS, AD–A054023.)
8. Daniel, I.M.; Shareef, I.; and Aliyu, A.A.: Rate Effects on Delamination Fracture Toughness of a Toughened Graphite/Epoxy. Toughened Composites, N.J. Johnston, ed., ASTM–STP–937, 1987, pp. 260–274.
9. Whitney, J.M.: Stress Analysis of the Double Cantilever Beam Specimen. Compos. Sci. Technol., vol. 23, no. 3, 1985, pp. 201–219.
10. Devitt, D.F.; Schapery, R.A.; and Bradley, W.L.: A Method for Determining the Mode I Delamination Fracture Toughness of Elastic and Viscoelastic Composite Materials. J. Compos. Mater., vol. 14, no. 4, 1980, pp. 270–285.
11. Gillespie, J.W., Jr.; Carlsson, L.A.; and Smiley, A.J.: Rate-Dependent Mode I Interlaminar Crack Growth Mechanisms in Graphite/Epoxy and Graphite/PEEK. Compos. Sci. Technol., vol. 28, no. 1, 1987, pp. 1–15.
12. Keary, P.E., et al.: Mode I Interlaminar Fracture Toughness of Composites Using Slender Double Cantilevered Beam Specimens. J. Compos. Mater., vol. 19, no. 2, 1985, pp. 154–177.
13. Berry, J.P.: Determination of Fracture Surface Energies by the Cleavage Technique. J. Appl. Phys., vol. 34, no. 1, 1963, pp. 62–68.
14. DeCharentenay, F.X., et al.: Characterizing the Effect of Delamination Defect by Mode I Delamination Test. Effects of Defects in Composite Materials, ASTM–STP–836, 1984, pp. 84–103.
15. Rice, J.R.: A Path Independent Integral and the Approximate Analysis of Strain Concentration by Notches and Cracks. J. Appl. Mech., vol. 35, no. 2, 1968, pp. 379–386.
16. Ashizawa, M.: Improving Damage Tolerance of Laminated Composites Through the Use of New Tough Resins. Proceedings of the 6th Conference on Fibrous Composites in Structural Design, AMMRC–MS–83–2, 1983, pp. IV–21 to IV–45 (Avail. NTIS, AD–P200010).
17. Bascom, W.D., et al.: The Interlaminar Fracture of Organic-Matrix, Woven Reinforcement Composites. Composites, vol. 11, no. 1, 1980, pp. 9–18.
18. Mostovoy, S.; Crosley, P.B.; and Ripling, E.J.: Use of Crack-Line-Loaded Specimens for Measuring Plane-Strain Fracture Toughness. J. Mater., vol. 2, no. 3, 1967, pp. 661–681.
19. Yaniv, G.; and Daniel, I.M.: Height-Tapered Double Cantilever Beam Specimen for Study of Rate Effects on Fracture-Toughness of Composites. Composite Materials: Testing and Design (Eighth Conference), J.D. Whitcomb, ed., ASTM–STP–972, 1988, pp. 241–258.
20. Hunston, D.L.; and Bascom, W.D.: Effects of Lay-up, Temperature, and Loading Rate in Double Cantilever Beam Tests of Interlaminar Crack Growth. Compos. Technol. Rev., vol. 5, no. 4, 1983, pp. 118–119.
21. Nicholls, D.J.; and Gallagher, J.P.: Determination of G_{Ic} in Angle Ply Composites Using a Cantilever Beam Test Method. J. Reinf. Plastics Compos., vol. 2, no. 1, 1983, pp. 2–17.
22. Ilcewicz, L.B.; Keary, P.E.; and Trostle, J.: Interlaminar Fracture Toughness Testing of Composite Mode I and Mode II DCB Specimens. Polym. Eng. Sci., vol. 28, no. 9, 1988, pp. 592–604.
23. Johnson, W.S.; and Mangalgiri, P.D.: Investigation of Fiber Bridging in Double Cantilever Beam Specimens. NASA TM–87716, 1986.
24. Russell, A.J.: Micromechanisms of Interlaminar Fracture and Fatigue. Polym. Compos., vol. 8, no. 5, 1987, pp. 342–351.
25. Su, K.B.: Mechanisms of Interlaminar Fracture in a Thermoplastic Matrix Composite Laminate. ICCM–V, Proc. 5th International Conference on Composite Materials, W.C. Harrigan, Jr., et al., eds., AIME, 1985, pp. 995–1006.
26. Bradley, W.L.; and Cohen, R.N.: Matrix Deformation and Fracture in Graphite-Reinforced Epoxies. Delamination and Debonding of Materials, W.S. Johnson, ed., ASTM–STP–876, 1985, pp. 389–410.
27. Phillips, D.C.; and Wells, G.M.: The stability of Transverse Cracks in Fibre Composites. J. Mater. Sci. Lett., vol. 1, no. 7, 1982 pp. 321–324.
28. Bradley, W.L.: Understanding the Translation of Neat Resin Toughness Into Delamination Toughness in Composites. Key Eng. Mater., vol. 37, 1989, pp. 161–198.
29. Gillespie, J.W., et al.: Delamination Growth in Composite Materials. NASA CR–178066, 1986.
30. Hunston, D.L., et al.: Matrix Resin Effects in Composite Delamination - Mode I Fracture Aspects. Toughened Composites, N.J. Johnston, ed., ASTM–STP–937, 1987, pp. 74–94.
31. Chai, H.: The Characterization of Mode I Delamination Failure in Non-Woven, Multidirectional Laminates. Composites, vol. 15, no. 4, 1984, pp. 277–290.
32. Ramkumar, R.L.; and Whitcomb, J.D.: Characterization of Mode I and Mixed-Mode Delamination Growth in T300/5208 Graphite/Epoxy. Delamination and Debonding of Materials, W.S. Johnson, ed., ASTM–STP–876, 1985, pp. 315–335.
33. Bascom, W.D., et al.: The Width-Tapered Double Cantilever Beam for Interlaminar Fracture Testing. Technology Vectors, 29th National SAMPE Symposium and Exhibition, SAMPE, 1984, pp. 970–978.
34. Jordan, W.M.; and Bradley, W.L.: The Relationship Between Resin Mechanical Properties and Mode I Delamination Fracture Toughness. J. Mater. Sci. Lett., vol. 7, no. 12, 1988, pp. 1362–1364.
35. Ting, R.Y.; and Cottington, R.L.: Comparison of Laboratory Techniques for Evaluating the Fracture Toughness of Glassy Polymers. J. Appl. Polym. Sci., vol. 25, no. 9, 1980, pp. 1815–1823.
36. Scott, J.M.; and Phillips, D.C.: Carbon Fibre Composites With Rubber Toughened Matrices. J. Mater. Sci., vol. 10, no. 4, 1975, pp. 551–562.
37. Mall, S.; Johnson, W.S.; and Everett, R.A., Jr.: Cyclic Debonding of Adhesively Bonded Composites. Adhesive Joints, K.L. Mittal, ed., Plenum Press, 1984, pp. 639–658.
38. Gales, R.D.R.; and Mills, N.J.: The Plane Strain Fracture of Polysulfone. Eng. Fract. Mech., vol. 6, no. 1, 1974, pp. 93–104.
39. Johnson, W.S.; and Mangalgiri, P.D.: Influence of the Resin on Interlaminar Mixed-Mode Fracture. Toughened Composites, N.J. Johnston, ed., ASTM–STP–937, 1987, pp. 295–315.
40. Corleto, C.R.; and Bradley, W.L.: Mode II Delamination Fracture Toughness of Unidirectional Graphite/Epoxy Composites. Composite Materials: Fatigue and Fracture, Vol. 2, P.A. Lagace, ed., ASTM–STP–1012, 1989, pp. 201–221.
41. Russell, A.J.: On the Measurement of Mode II Interlaminar Fracture Energies. DREP–82–0, Dec. 1982 (Avail. NTIS, AD–B078085).
42. Russell, A.J.; and Street, K.N.: Moisture and Temperature Effects on the Mixed-Mode Delamination Fracture of Unidirectional Graphite/Epoxy. Delamination and Debonding of Materials, W.S. Johnson, ed., ASTM–STP–876, 1985, pp. 349–370.

43. Mall, S.; and Kochhar, N.K.: Finite-Element Analysis of End-Notch Flexure Specimens. J. Compos. Technol. Res., vol. 8, no. 2, 1986, pp. 54–57.
44. Carlsson, L.A.; Gillespie, J.W., Jr.; and Pipes, R.B.: On the Analysis and Design of the End Notched Flexure (ENF) Specimen for Mode II Testing. J. Compos. Mater., vol. 20, no. 6, 1986, pp. 594–604.
45. Prel, Y., et al.: Mode I and Mode II Delamination of Thermosetting and Thermoplastic Composite. Composite Materials: Fatigue and Fracture, Vol. 2, P.A. LaGrace, ed., ASTM–STP–1012, 1989, pp. 251–269.
46. Carlsson, L.A.; Gillespie, J.W.; and Trethewey, B.R.: Mode II Interlaminar Fracture of Graphite/Epoxy and Graphite/PEEK. J. Reinf. Plastics Compos., vol. 5, no. 3, 1986, pp. 170–187.
47. O'Brien, T.K.; Murri, G.B.; and Salpekar, S.A.: Interlaminar Shear Fracture Toughness and Fatigue Thresholds for Composite Materials. Composite Materials: Fatigue and Fracture, vol. 2, P.A., LaGrace, ed., ASTM–STP–1012, 1989, pp. 222–250.
48 Gillespie, J.W., Jr.; Carlsson, L.A.; and Pipes, R.B.: Finite Element Analysis of the End Notched Flexure Specimen for Measuring Mode II Fracture Toughness. Compos. Sci. Technol., vol. 27, no. 3, 1986, pp. 177–197.
49. Russell, A.J.; and Street, K.N.: The Effect of Matrix Toughness on Delamination – Static and Fatigue Fracture Under Mode II Shear Loading of Graphite Fiber Composites. Toughened Composites, N.J. Johnston, ed., ASTM–STP–937, 1987, pp. 275–294.
50. Wilkins, D.J.: A Comparison of the Delamination and Environmental Resistance of a Graphite-Epoxy and a Graphite-Bismaleimide. NAV–GD–0037, Sept. 1981 (Avail. NTIS, AD–A1122474).
51. Mall, S.; and Johnson, W.S.: Characterization of Mode I and Mixed-Mode Failure of Adhesive Bonds Between Composite Adherends. Composite Materials: Testing and Design (Seventh Conference), J.M. Whitney, ed., ASTM–STP–893, 1986, pp. 322–334.
52. Dattaguru, B., et al.: Geometrically Nonlinear Analysis of Adhesively Bonded Joints. J. Eng. Mater. Technol., vol. 106, no. 1, 1984, pp. 59–65.
53. Rybicki, E.F.; and Kanninen, M.F.: A Finite Element Calculation of Stress Intensity Factors by a Modified Crack Closure Integral. Eng. Fract. Mech., vol. 9, no. 4, 1977, pp. 931–938.
54. Mangalgiri, P.D.; and Johnson, W.S.: ASTM D–30.02.02 Meeting, Dallas, TX, 1984.
55. Puppo, A.H.; and Evensen, H.A.: Interlaminar Shear in Laminated Composites Under Generalized Plane Stress. J. Compos. Mater., vol. 4, no. 2, 1970, pp. 204–220.
56. Pipes, R.B.; and Pagano, N.J.: Interlaminar Stresses in Composite Laminates Under Unifrom Axial Extension. J. Compos. Mater., vol. 4, no. 4, 1970, pp. 538–548.
57. Pagano, J.J.; and Pipes, R.B.: Some Observations on the Interlaminar Strength of Composite Laminates. Int. J. Mech. Sci., vol. 15, no. 8, 1973, pp. 679–692.
58. Wang, A.S.D.: An Overview of the Delamination Problem in Structural Composites. Key Eng. Mater., vol. 37, no. 1, 1989, pp. 1–20.
59. O'Brien, T.K.: Characterization of Delamination Onset and Growth in a Composite Laminate. Damage in Composite Materials, K.L. Reifsnider, ed., ASTM–STP–775, 1982, pp. 140–167.
60. O'Brien, T.K., et al.: Simple Test for the Interlaminar Fracture Toughness of Composites. SAMPE J., vol. 18, no. 4, 1982, pp. 8–15.
61. O'Brien, T.K., et al.: Comparisons of Various Configurations of Edge Delamination Test for Interlaminar Fracture Toughness. Toughened Composites, N.J. Johnston, ed., ASTM–STP–937, 1987, pp. 199–221.
62. O'Brien, T.K.: Mixed-Mode Strain-Energy-Release Rate Effects on Edge Delamination of Composites. Effects of Defects in Composite Materials, ASTM–STP–836, 1984, pp. 125–142.
63. Whitney, J.M.; and Knight, M.: A Modified Free-Edge Delamination Specimen. Delamination and Debonding of Materials, W.S. Johnson, ed., ASTM–STP–876, 1985, pp. 298–314.
64. Law, G.E.: A Mixed-Mode Fracture Analysis of (±25/90 n)s Graphite/Epoxy Composite Laminates. Effects of Defects in Composite Materials, ASTM–STP–836, 1984, pp. 143–160.
65. Wang, S.S.; and Mandell, J.F.: Analysis of Delamination in Unidirectional and Crossplied Fiber Composites Containing Surface Cracks. NASA CR–135248, 1977.
66. Wang, S.S.: Delamination Crack Growth in Unidirectional Fiber-Reinforced Composites Under Static and Cyclic Loading. Composite Materials: Testing and Design, S.W. Tsai, ed., ASTM–STP–674, 1979, pp. 642–663.
67. Jurf, R.A.; and Pipes, R.B.: Interlaminar Fracture of Composite Materials. J. Compos. Mater., vol. 16, no. 3, 1982, pp. 386–394.
68. Daniel, I.M.; and Aliyu, A.A.: Effects of Strain Rate on Delamination Fracture Toughness of Graphite/Epoxy. Delamination and Debonding of Materials, W.S. Johnson, ed., ASTM–STP–876, 1985, pp. 336–348.
69. Williams, J.H., Jr.; Lee, S.S.; and Kousiounelos, P.N.: Dynamic Crack Propagation and Arrest in Orthotropic DCB Fiber Composite Specimens. Eng. Fract. Mech., vol. 14, no. 2, 1981, pp. 427–438.
70. de Charentenay, F.X.; and Benzeggagh, M.: Fracture Mechanics of Mode I Delamination in Composite Materials. Advances in Composite Materials, Vol. 1, A.R. Bunsell, et al., eds., Pergamon Press, 1980, pp. 186–197.
71. Bitner, J.L., et al.: Viscoelastic Fracture of Structural Adhesives. J. Adhesion, vol. 13, no. 1, 1981, pp. 3–28.
72. Miller, A.G.; Hertzberg, P.E.; and Rantala, V.W.: Toughness Testing of Composite Materials. Materials 1980, SAMPE, 1980, pp. 279–293 (Also as; SAMPE Q., vol. 12, no. 1, 1981, pp. 36–42).
73. Sun, C.T.; and Grady, J.E.: Dynamic Delamination Crack Propagation in a Graphite/Epoxy Laminate. Composite Materials: Fracture and Fatigue, H.T. Hahn, ed., ASTM–STP–907, 1986, pp. 5–31.
74. Sun, C.T.; and Grady, J.E.: Dynamic Delamination Fracture Toughness of a Graphite/Epoxy Laminate Under Impact. Compos. Sci. Technol., vol. 31, no. 1, 1988, pp. 55–72.
75. Chang, T.D.; and Brittain, J.O.: Studies of Epoxy Resin Systems: Part D: Fracture Toughness of an Epoxy Resin: A Study of the Effect of Crosslinking and Sub-T_g Aging. Polym. Eng. Sci., vol. 22, no. 12, 1982, pp. 1228–1236.
76. Klein, A.J.: Building Tough Composites. Adv. Mater. Processes, vol. 1, no. 2, 1985, pp. 43–46.
77. Yee, A.F.: Modifying Matrix Materials for Tougher Composites. Toughened Composites, N.J. Johnston, ed., ASTM–STP–937, 1987, pp. 383–396.
78. Krieger, R.B., Jr.: Advances in Toughness of Structural Composites Based on Interleaf Technology. Progress in Advanced Materials and Processes: Durability, Reliability and Quality Control, G. Bartelds and R.J. Schliekelmann, eds., Elsevier, 1985, pp. 189–199.
79. Masters, J.E.; Courter, J.L.; and Evans, R.E.: Impact Fracture and Failure Suppression Using Interleafed Composites. Materials Sciences for the Future, J.L. Bauer and R. Dunaetz, eds., SAMPE, 1986, pp. 844–858.
80. Masters, J.E.: Improved Impact and Delamination Resistance Through Interleading. Key Eng. Mater., vol. 37, 1989, pp. 317–348.
81. Hirschbuehler, K.R.: A Comparison of Several Mechanical Tests Used to Evaluate the Toughness of Composites. Toughened Composites, N.J. Johnston, ed., ASTM–STP–937, 1987, pp. 61–73.
82. Ishai, O., et al.: Effect of Selective Adhesive Interleaving on Interlaminar Fracture Toughness of Graphite/Epoxy Composite Laminates. Composites, vol. 19, no. 1, 1988, pp. 49–54.
83. Browning, C.E.; and Schwartz, H.S.: Delamination Resistant Composite Concepts. Composite Materials: Testing and Design (Seventh Conference), J.M. Whitney, ed., ASTM–STP–893, 1986, pp. 256–265.
84. Chan, W.S.: Delamination Arrester – An Adhesive Inner Layer in Laminated Composites. Composite Materials: Fatigue and Fracture, H.T. Hahn, ed., ASTM–STP–907, 1986, pp. 176–196.
85. Hibbs, M.F.; Bradley, W.L.; and Tse, M.K.: Interlaminar Fracture Toughness and Real-Time Fracture Mechanism of Some Toughened Graphite/Epoxy Composites. Toughened Composites, N.J. Johnston, ed., ASTM–STP–937, 1987, pp. 115–130.

86. Broutman, L.J.; and Agarwal, B.D.: Theoretical Study of Effect of an Interfacial Layer on Properties of Composites. Polym. Eng. Sci., vol. 14, no. 8, 1974, pp. 581–588.
87. Peiffer, D.G.; and Nielsen, L.E.: Preparation and Mechanical Properties of Thick Interlayer Composites. J. Appl. Polym. Sci., vol. 23, no. 8, 1979, pp. 2253–2264.
88. Joseph, R.; Bell, J.P.; and Rhee, H.: Fracture Behavior of Coated/ Uncoated Graphite-Epoxy Composites. Polym. Eng. Sci., vol. 28, no. 9, 1988, pp. 605–609.
89. Bell, J.P., et al.: Application of Ductile Polymeric Coatings onto Graphite Fibers. Polym. Compos., vol. 8, no. 2, 1987, pp. 46–52.
90. Schwartz, H.S.; and Hartness, J.T.: Effect of Fiber Coatings on Interlaminar Fracture Toughness of Composites. Toughened Composites, N.J. Johnston, ed., ASTM–STP–937, 1987, pp. 150–165.

Appendix A

Symbols

A	crack surface area
A_0,A_1,A_3	curve fit parameters
a	crack length
a_c	extension of existing crack covered by P_c
á	crack propagation speed
B	specimen width
C	compliance
C_o	uncracked compliance
D	energy dissipated through fracture
E	flexural modulus
$E = E_{11}$	modulus in fiber direction
$E = E_{11}$	stiffness in fiber direction
E*	laminate stiffness in loading direction
E_i	longitudinal modulus
E_{lam}	stiffness before delamination
E_1/E_2	material orthotropy ratio
G	energy release rate
G_I	mode I energy release rate
G_{II}	mode II energy release rate
G_{Ic}	mode I fracture toughness
G_{IIc}	mode II fracture toughness
G_c	critical energy release rate
G_{12}	in-plane shear modulus
G_{13}	transverse shear modulus
h	test specimen thickness
h_1,h_2	thickness of two sections of test specimen
J	measure of energy available for crack extension: J = G for elastic deformation
K	curve-fitting parameter
k	taper ratio
L	test specimen length
m	curve fit parameter
n	curve fit parameter
P	load
P_c	critical load
R	fracture resistance of materials
S	shear compliance
T	kinetic energy
t	thickness
U	strain energy
W	external work done by applied load
y´	slope
α	curve fit parameter
β	curve fit parameter
ΔA	area between loading and unloading curves
Δa	crack extension
δ	load point displacement
δ_c	critical displacement
ε	strain
ε_c	critical strain level

θ	rotation
μ	coefficient of friction
σ_{xy}	in-plane shearing stress
σ_{xz}	out-of-plane shearing stress
σ_y	normal stress

Subscripts:

c	critical
eff	effective

Superscripts:

FE	finite element
BT	beam theory

Appendix B

Tables

TABLE I. – MODE I INTERLAMINAR FRACTURE TOUGHNESS MEASUREMENTS

Fiber/Matrix	Test	Delamination interface degree/degree	Fiber content, vol, %	G_{Ic}, (J/m^2)	Reference
985					
T300/985	DCB	0/0	56	128	12
914					
T300/914	DCB		55	185	45
3502			0	69	26
3502			0	70	34
AS1/3502	DCB			155	26
AS4/3502	DCB			190	28
AS4/3502	DCB		76	225	26
5208	WTDCB		0	76	17
5208			0	80	30
T300/5208	DCB		56	84	22
T300/5208	DCB	+45/-45	72	84	31
T300/5208	DCB	0/45	72	86	31
T300/5208	DCB	0/0	68	88	5
T300/5208	DCB		65	100	30
T300/5208	DCB			103	32
Dow P4			0	80	28
AS4/Dow P4	DCB			160	28
3501-6			0	70	28
3501-6			0	95	30
AS1/3501-6	DCB		62	110	24
AS4/3501-6	DCB			144	28
AS4/3501-6	DCB		67	175	30
2220-3			0	95	33
AS4/2220-3	DCB		61	160	24
AS4/2220-3	DCB			221	16
AS6/2220-3	DCB		57	238	22
AS4/2220-3	DCB			250	33
Dow P6			0	150	28
AS4/Dow P6	DCB			160	28
3100					
T300/3100	DCB			170	37
DGEBA					
Glass/DGEBA	DCB		60	264	45
5245c					
AS6/5245c	DCB		57	287	22
PMR-15					
C6000/PMR-15	DCB		66	294	22
F-155 NR[a]			0	167	34
AS4/F-155 NR	DCB		54	335	28
Hx205			0	230	35
Hx205	WTDCB		0	270	17
Hx205	WTDCB		0	340	28

[a]F-155 epoxy without carboxy-terminated butadiene acrylonitride (CTBN) additive

TABLE I. – MODE I INTERLAMINAR FRACTURE TOUGHNESS MEASUREMENTS (Continued)

Fiber/Matrix	Test	Delamination interface degree/degree	Fiber content, vol, %	G_{Ic}, (J/m^2)	Reference
T300/Hx205	DCB		58	380	30
C6000/Hx205	DCB	0/0		455	28
T300/Hx205	WTDCB	b	61	600	17
C6000/Hx205	DCB		56	790	30
Glass/Hx205	WTDCB	c	60	1000	17
BP907			0	325	28
T300/BP907	DCB	0/0	56	292	12
T300/BP907	DCB	0/45	62	333	31
T300/BP907	DCB	0/0		380	28
T300/BP907	DCB	0/0	62	382	31
T300/BP907	DCB	0/90	62	390	31
T300/BP907	DCB	+45/-45	62	403	31
MY750[d]	WTDCB		0	330	36
MY750[e]	WTDCB		0	1400	36
MY750[f]	WTDCB		0	2200	36
MY750[g]	WTDCB		0	3200	36
AS4/MY750[d]	WTDCB	0/0	60	280	36
AS4/MY750[e]	WTDCB		60	370	36
AS4/MY750[f]	WTDCB		60	360	36
AS4/MY750[g]	WTDCB		60	490	36
F-185 NR[h]			0	460	34
AS4/F-185 NR	DCB		58	455	34
R6376					
IM-6/R-6376	DCB			473	37
F-155			0	730	34
C6000/F-155	DCB		51	495	24
AS4/F-155	DCB		69	520	24
C6000/F-155	DCB			600	26
AS4/F-155	DCB		60	1015	34
Hx206			0	2200	35
T300/Hx206	DCB		55	830	30
C6000/Hx206	DCB			1200	28
C6000/Hx206	DCB		49	1550	30
Hx210			0	2800	28
C6000/Hx210	DCB			1800	28
F-263					
T300/F-263	DCB		56	119	12
T300/F-263	WTDCB	b	64	360	17
P-1700			0	2500	30
T300/P-1700	DCB	0/0	52	1200	30
P-1700	WTDCB		0	3200	38
PEEK[i]					
AS4/PEEK	DCB	0/0	58	1147	22
AS4/PEEK	DCB	0/0		1205	37
AS4/PEEK	DCB	0/0	66	1330	24

[b]13×12 weave
[c]7781 S-glass, 8HS weave
[d]Unmodified epoxy
[e]MY750+3.2 percent CTBN rubber
[f]MY750+6.2 percent CTBN rubber
[g]MY750+9.0 percent CTBN rubber
[h]F-185 epoxy without CTBN additive
[i]Thermoplastic

TABLE I. – MODE I INTERLAMINAR FRACTURE TOUGHNESS MEASUREMENTS (Concluded)

Fiber/Matrix	Test	Delamination interface degree/degree	Fiber content, vol, %	G_{Ic}, (J/m^2)	Reference
AS4/PEEK	DCB	0/0	61	1460	45
AS4/PEEK	DCB	0/0		1751	11
Ultem-1000[i]			0	3300	30
T300/Ultem	DCB	0/0	65	935	30
T300/Ultem	DCB	0/0	60	1060	30
F-185	WTDCB		0	5100	17
F-185			0	5830	35
F-185			0	6400	28
F-185			0	8000	34
T300/F-185	DCB	0/0	59	1960	30
AS4/F-185	DCB	0/0	57	2200	28
C6000/F-185	DCB		57	2250	30
C6000/F-185	DCB			2700	26
Glass/F-185	WTDCB	c	60	4400	17
T300/F-185		b	58	4600	17
Lexan			0	8100	28
AS4/Lexan	DCB	0/0		1600	28

[b]13×12 weave
[c]7781 S-glass, 8HS weave
[i]Thermoplastic

TABLE II. – MODE II INTERLAMINAR FRACTURE TOUGHNESS MEASUREMENTS

Fiber/Matrix	Test	Delamination interface degree/degree	Fiber content, vol, %	G_{Ic}, (J/m^2)	Reference
3501-6					
AS1/3501-6	ENF	0/90		370	41
AS1/3501-6	ENF	0/45		438	41
AS1/3501-6	ENF	0/0		444	41
AS1/3501-6	ENF		62	605	24
AS4/3501-6	ENF			1150	28
914					
T300/914	ENF		55	518	45
3100					
T300/3100	ENF			548	37
3502					
AS4/3502	ELS			543	40
AS4/3502				570	28
AS4/3502	ENF			615	40
F-263					
T300/F-263	ELS		56	594	22
R-6376					
IM-6/R-6376	ENF			650	37
985					
T300/985	ELS		56	697	22
5208					
T300/5208	ELS		56	716	22
T300/5208	ENF			865	47
2220-3					
AS4/2220-3	ENF		61	750	24
AS6/2220-3	ELS		57	968	22
Dow P4					
AS4/Dow P4				800	28
F-155					
C6000/F-155	ENF		51	900	24
AS4/F-155				1500	28
5245c					
AS6/5245c	ELS		57	977	22
F-185 NR[a]					
AS4/F-185 NR				1050	28
BP907					
T300/BP907	ELS		56	1423	22
T300/BP907	ENF			2627	47
F-155 NR[b]					
AS4/F-155 NR				1660	28
Lexan					
AS4/Lexan				1700	28

[a]F-185 epoxy without CTBN additive
[b]F-155 epoxy without CTBN additive

TABLE II. – MODE II INTERLAMINAR FRACTURE TOUGHNESS MEASUREMENTS (Concluded)

Fiber/Matrix	Test	Delamination interface degree/degree	Fiber content, vol, %	G_{Ic}, (J/m^2)	Reference
DGEBA					
Glass/DGEBA	ENF	0/0	60	1715	45
Glass/DGEBA	ELS		60	2110	45
Dow P6					
AS4/Dow P6				1750	28
PEEK[c]					
AS4/PEEK	ENF		61	1109	45
AS4/PEEK	ENF			1502	37
AS4/PEEK				1700	11
AS4/PEEK	ENF		66	1765	24
AS4/PEEK	ELS		61	1780	45
AS4/PEEK	ELS		58	2425	22
F-185					
AS4/F-185	ELS			2265	40
AS4/F-185	ENF			2354	40

[c]Thermoplastic

TABLE III. – MODE III INTERLAMINAR FRACTURE TOUGHNESS MEASUREMENTS

Fiber/Matrix	Test	Delamination interface degree/degree	$\frac{G_I}{G_{II}}$	G_{Ic}, (J/m^2)	Reference
5208					
T300/5208	EDT	0/0	1.33	84	59
T300/5208	CLS	45/45	0.29	460	32
Dow P4					
AS4/Dow P4		0/0	1.33	160	28
Dow P6					
AS4/Dow P6			1.33	160	28
3100					
T300/3100	CLS			170	37
3501-6					
AS4/3501-6			1.33	175	28
DGEBA					
Glass/DGEBA	a		1.14	264	45
Hx205					
AS4/Hx205			1.33	380	28
C6000/Hx205	EDT		1.33	790	59
R-6376					
IM-6/R-6376	CLS			473	37
F-155					
AS4/F-155			1.33	495	28
PEEK[b]					
AS4/PEEK	CLS			1147	37
F-185					
C6000/F-185	EDT		1.38	5830	59

[a]Test described in ref. 45
[b]Thermoplastic

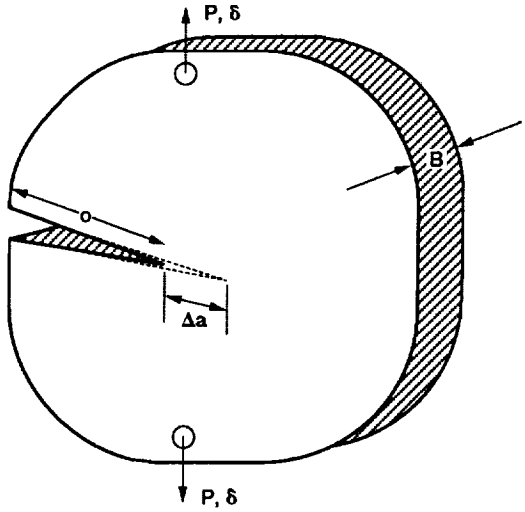

Figure 1.—Cracked structure under load (adapted from ref. 2).

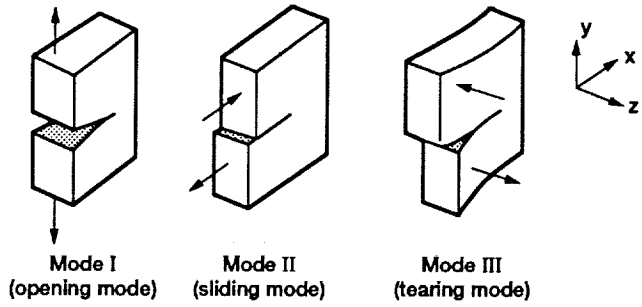

Figure 2.—Fracture modes (adapted from ref. 2).

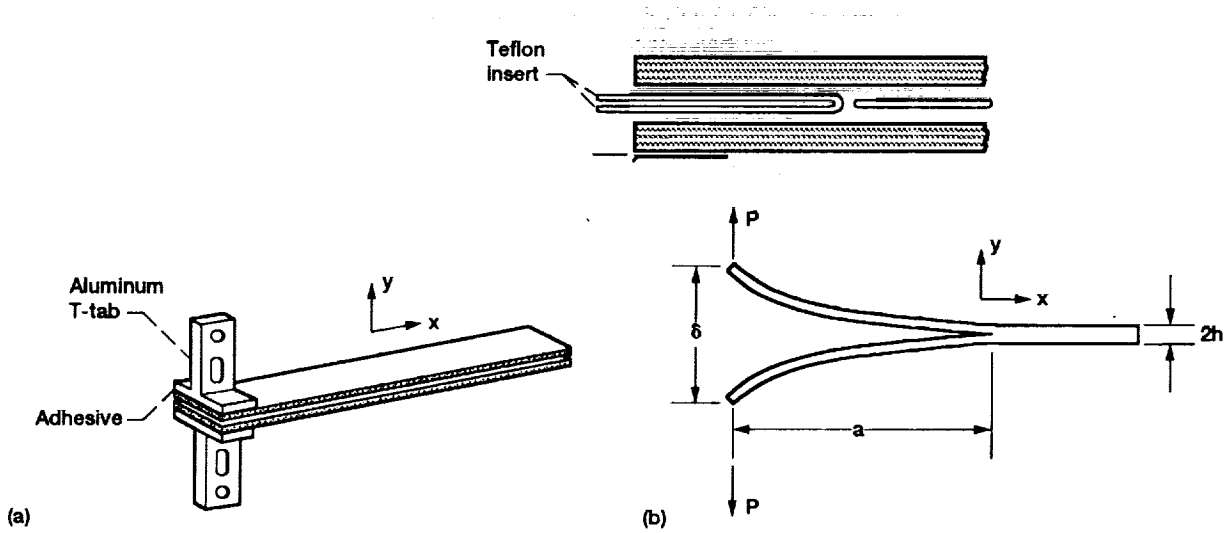

(a) Test specimen geometry.
(b) Deformed shape.

Figure 3.—Double cantilever beam specimen (adapted from refs. 4 and 5).

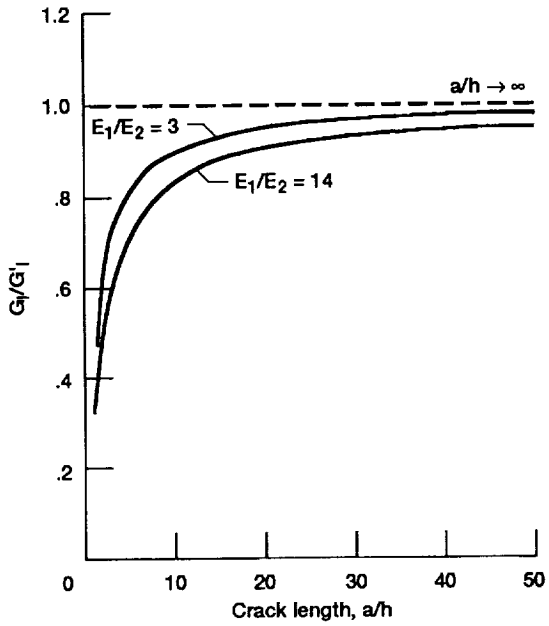

Figure 4.—Energy release rate correction for beam theory (adapted from ref. 9). $G_{12}/E_2 = 0.53$; $\nu_{12} = 0.3$; $\nu_{23} = 0.55$; K = 5/6.

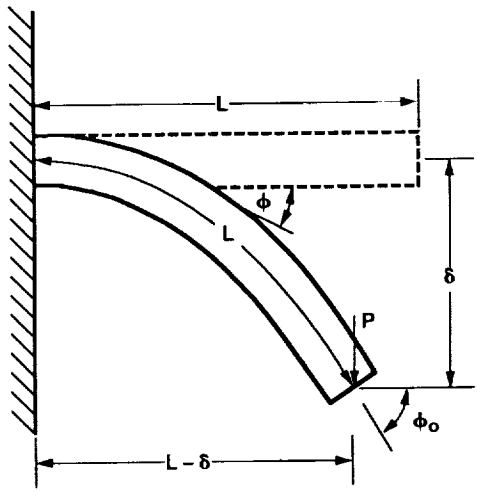

Figure 5.—Large displacement of cantilever beam (adapted from ref. 10).

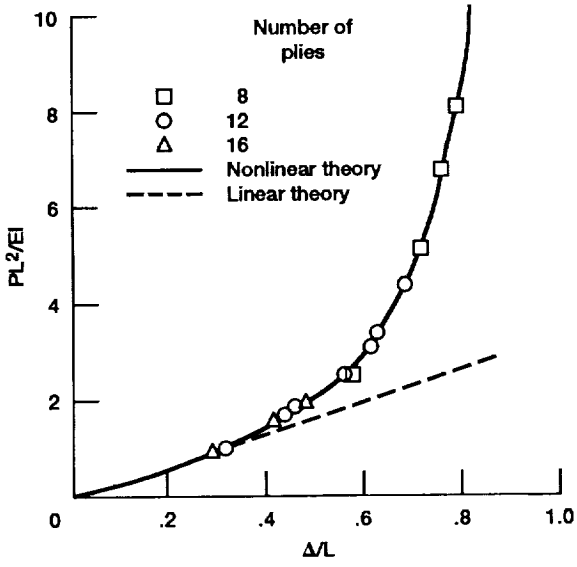

Figure 6.—Nonlinear beam theory is required for δ/a ≥ 0.3 (adapted from ref. 10).

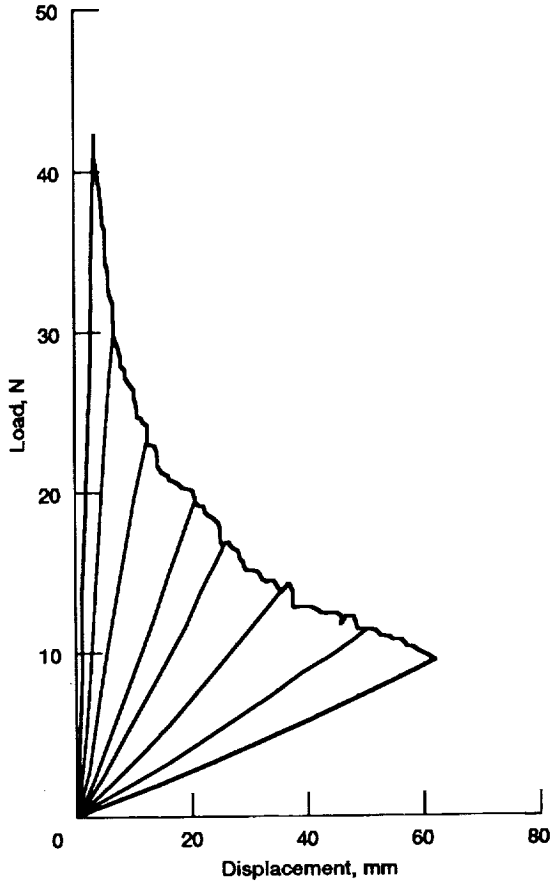

Figure 7.—Typical results from a DCB test of a brittle-matrix composite showing successive loading/crack extension/unloading cycles (adapted form ref. 11).

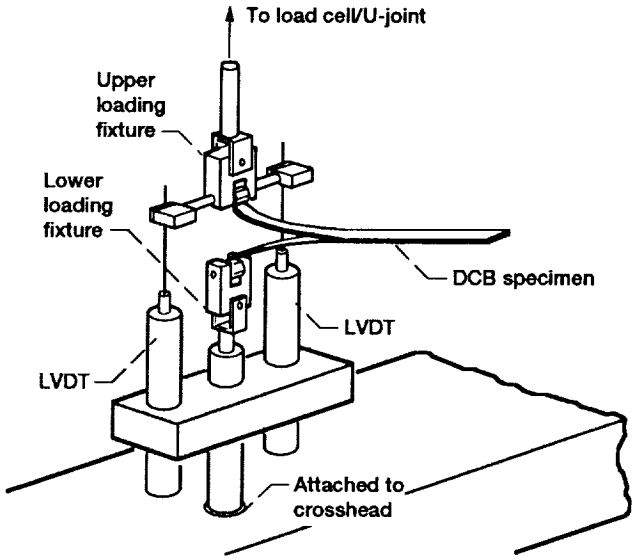

Figure 8.—Typical configuration for a double cantilever beam test by beam analysis method (adapted from ref. 12).

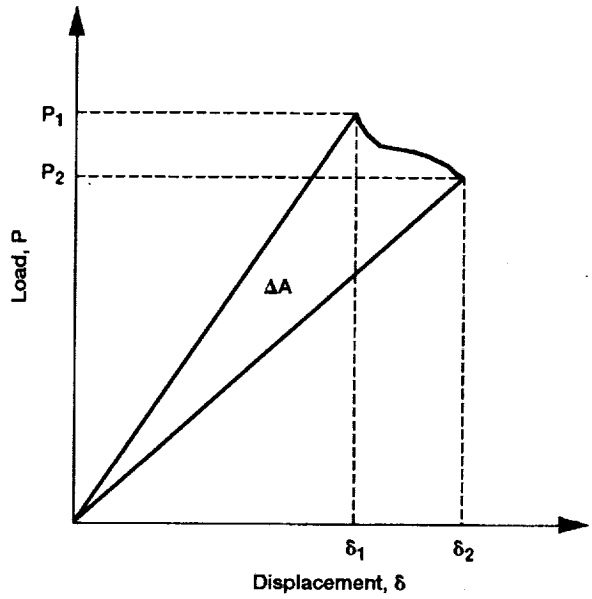

Figure 9.—A single loading-unloading curve for a brittle material (adapted from ref. 4).

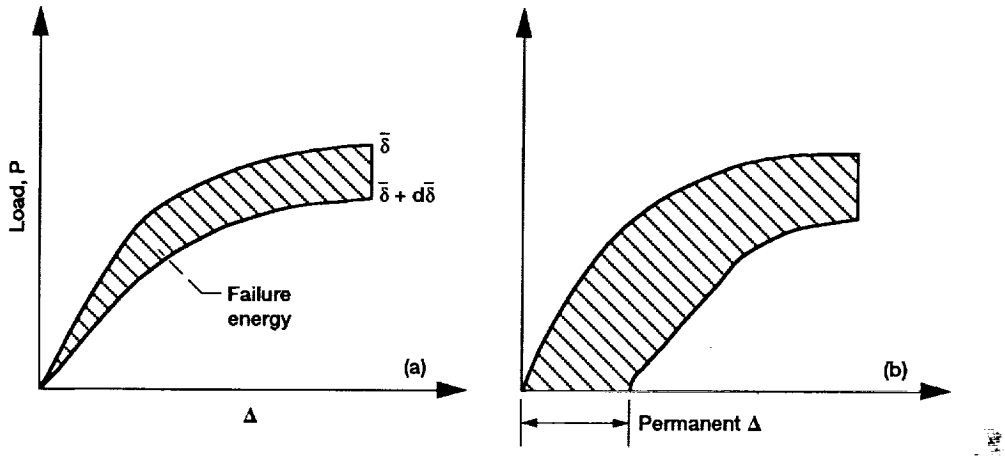

(a) Actual fracture energy.
(b) Area method calculation.

Figure 10.—Nonlinear load-displacement behavior with inelastic deformation (adapted from ref. 12).

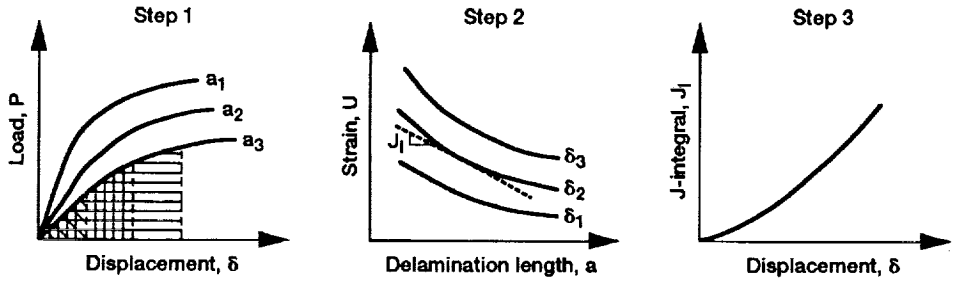

Figure 11.—Experimental procedure for J-integral calculation (adapted form ref. 12).

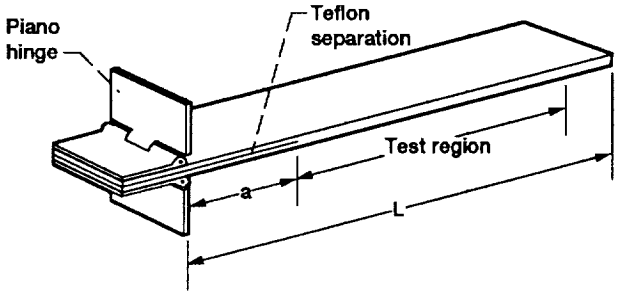

Figure 12.—Hinged double cantilever beam (adapted from ref. 16). a = delamination length; L = specimen length.

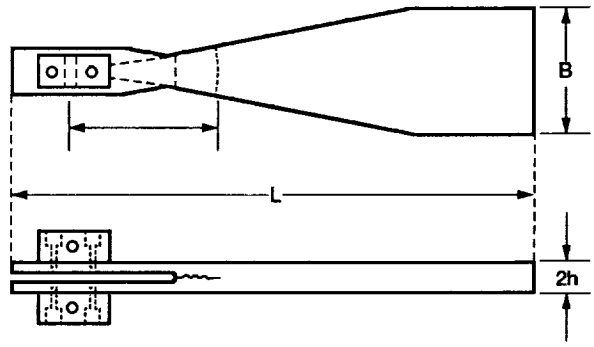

Figure 13.—Width-tapered double cantilever beam (adapted from ref. 17).

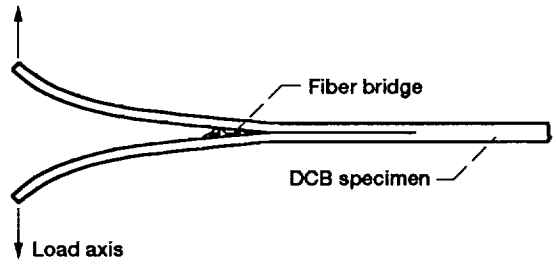

Figure 14.—Fiber bridging in DCB specimen (adapted from ref. 22).

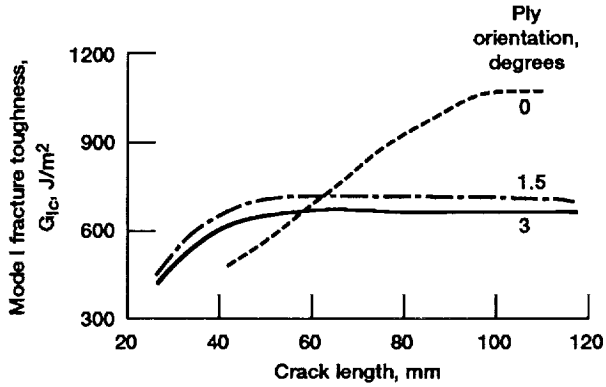

Figure 15.—R-curve behavior in toughened-matrix composite (C6000/Hx205) due to fiber bridging (adapted from ref. 23).

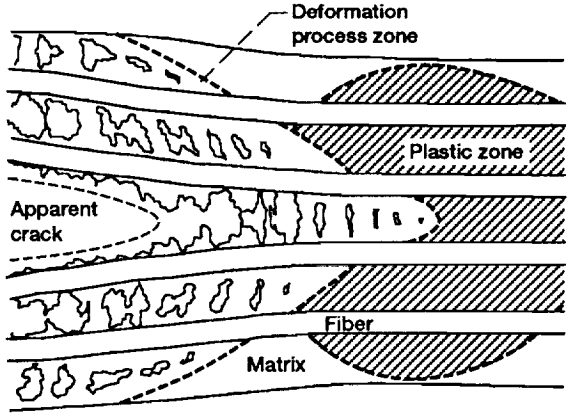

Figure 16.—Crack-tip process zone in toughened composite (adapted from ref. 25).

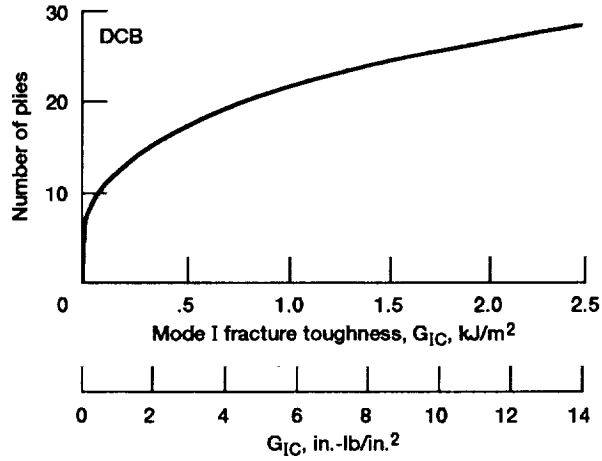

Figure 17.—Minimum DCB specimen thickness required to maintain linear elastic behavior (adapted from ref. 29). a = 152.4 mm (6 in.); E = 138 GPa (20 x 10^6 psi).

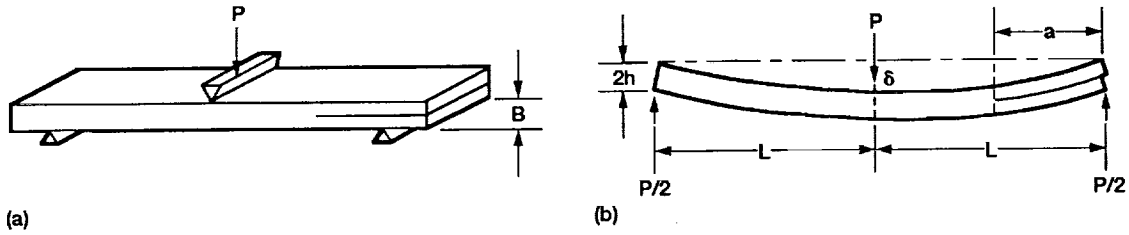

(a) Test specimen geometry.
(b) Deformed shape.

Figure 18.—End-notched flexure specimen (adapted from ref. 39, 40).

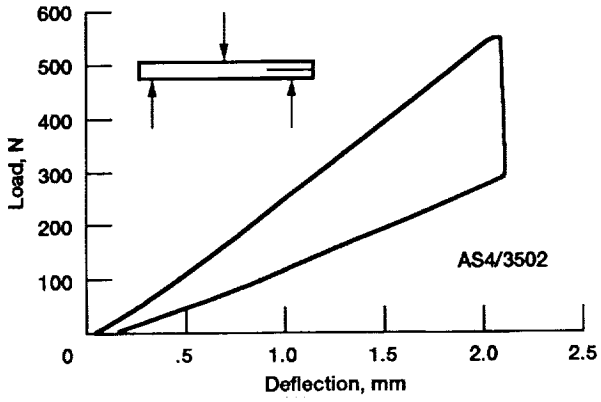

Figure 19.—Linear elastic behavior of a brittle AS4/3502 ENF specimen (adapted from ref. 40).

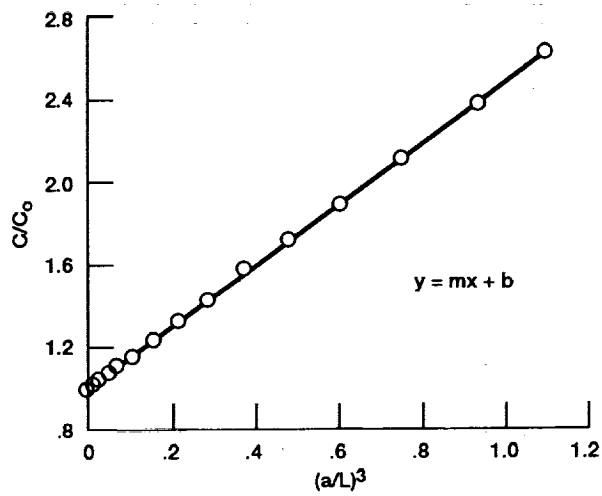

Figure 20.—Compliance calibration curve for a $[0]_{26}$ AS4/3501-6 ENF specimen (adapted from ref. 46). Slope (m) = 1.5105, intercept (b) = 1.0027.

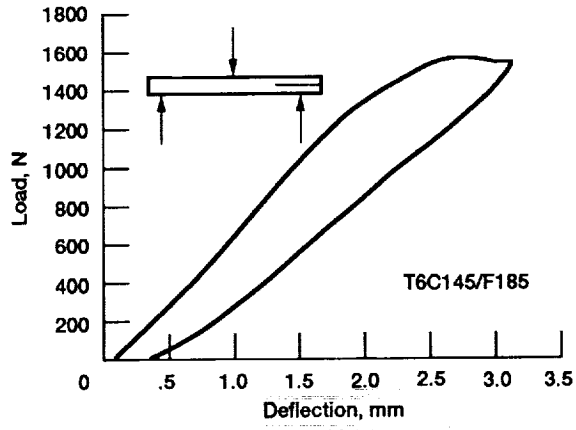

Figure 21.—Nonlinear elastic behavior of a toughened AS4/F-185 ENF specimen (adapted from ref. 40).

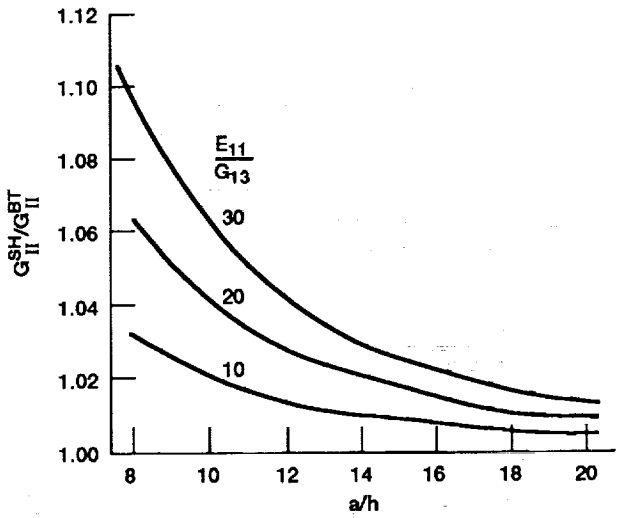

Figure 22.—Effect of shear compliance on beam theory calculation of G_{II} from an ENF test.

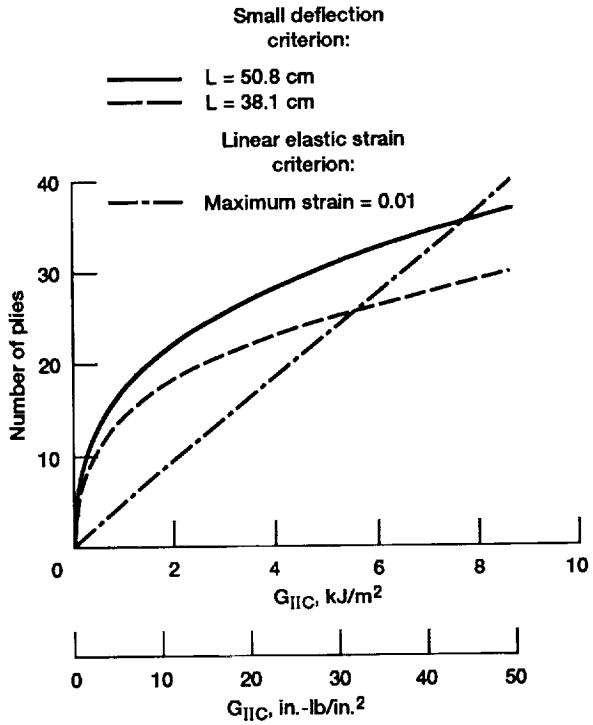

Figure 23.—Minimum ENF specimen thickness required to maintain linear elastic behavior (adapted from ref. 44).

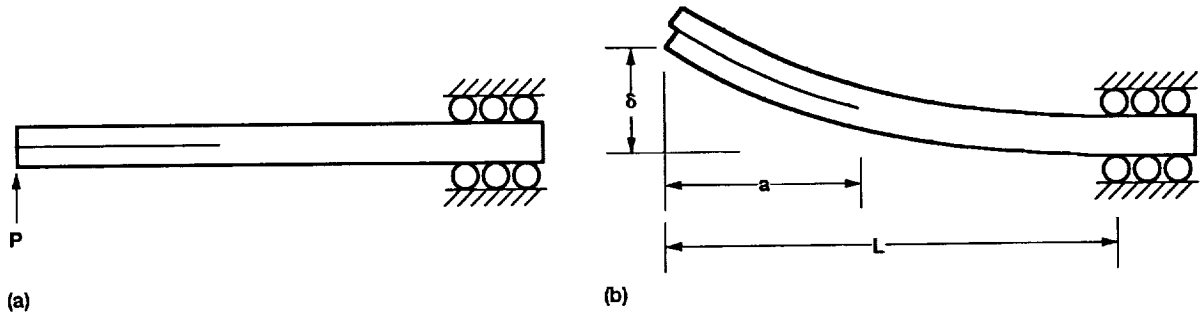

(a) Test specimen geometry.
(b) Deformed shape.

Figure 24.—End-loaded split test specimen.

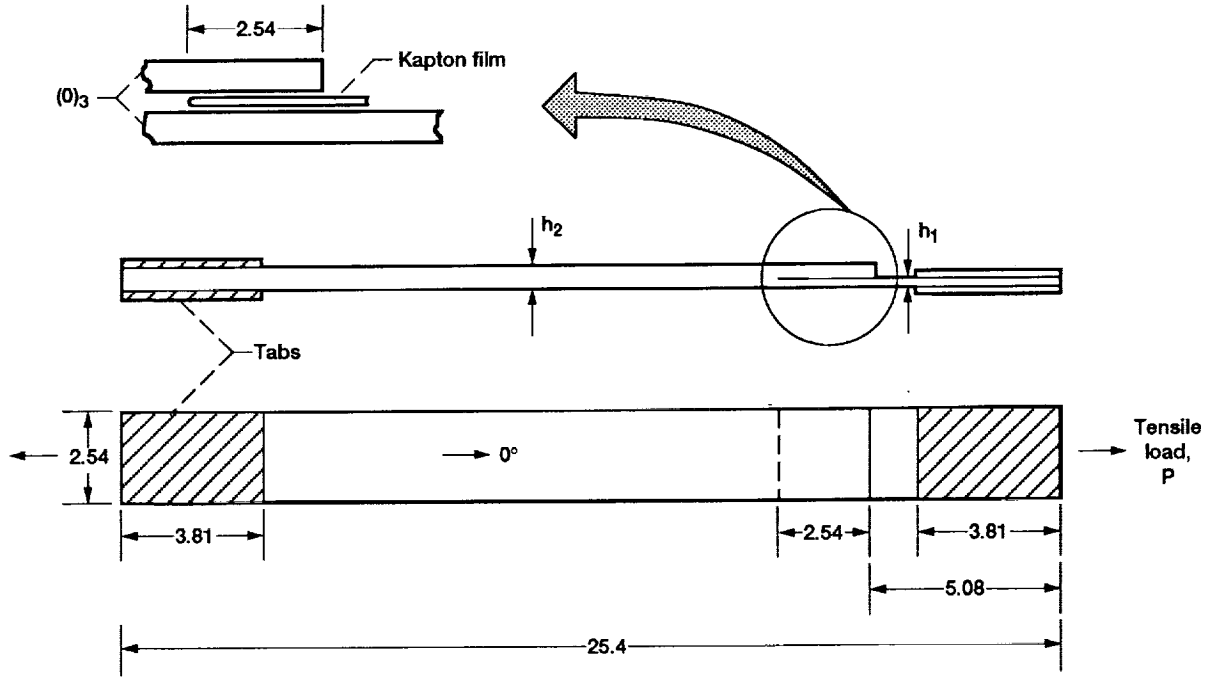

Figure 25.—Cracked-lap shear test specimen (adapted from ref. 50); all dimensions in centimeters.

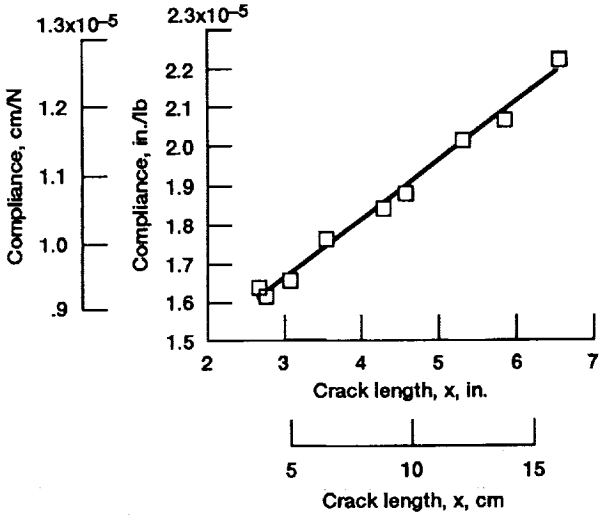

Figure 26.—Compliance calibration curve for CLS specimen (adapted from ref. 50).

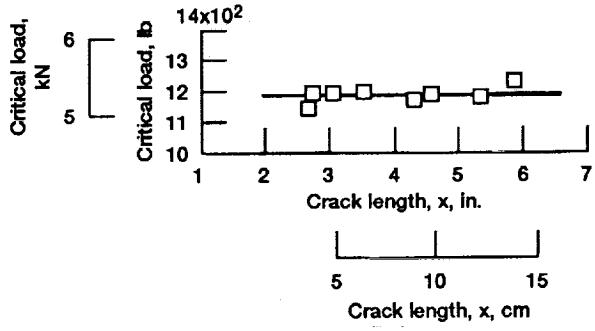

Figure 27.—Critical load for CLS test is independent of crack length (adapted from ref. 50).

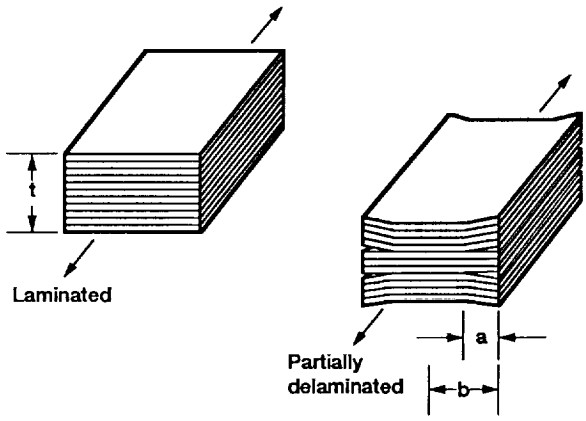

Figure 28.—Edge-delamination test specimen before and after onset of delamination (adapted from ref. 59).

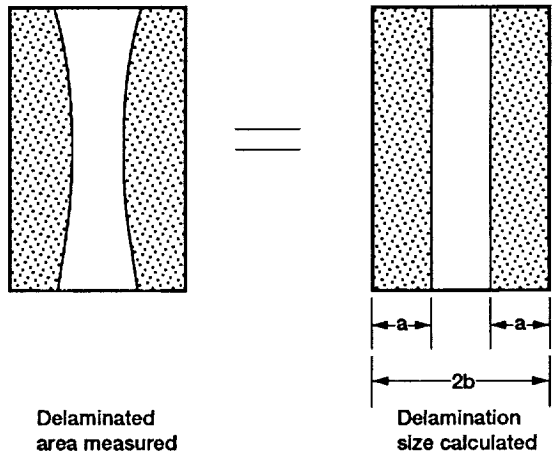

Figure 29.—Idealization of edge-delamination shape for calculation of equivalent crack length (adapted from ref. 59).

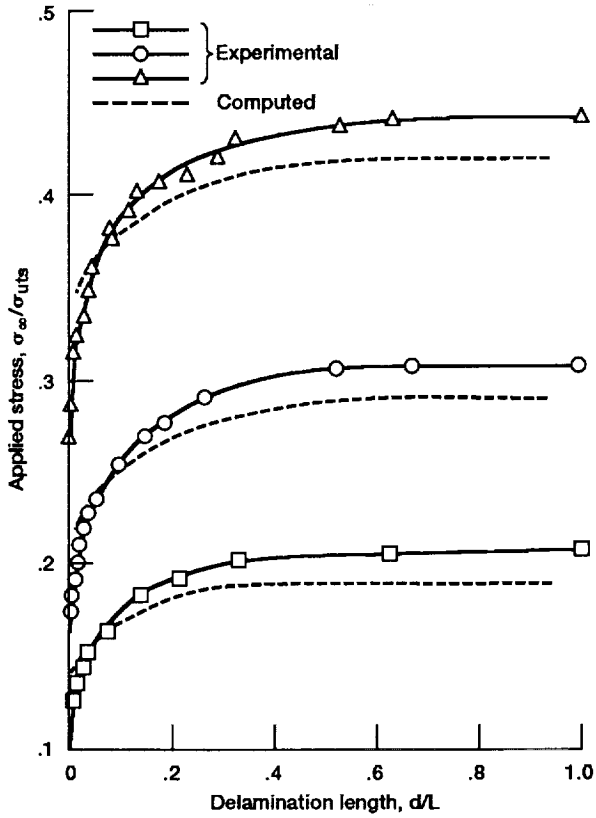

Figure 30.—Mixed-mode delamination growth calculated with total energy release rate criterion at three different ply interfaces (adapted from ref. 66).

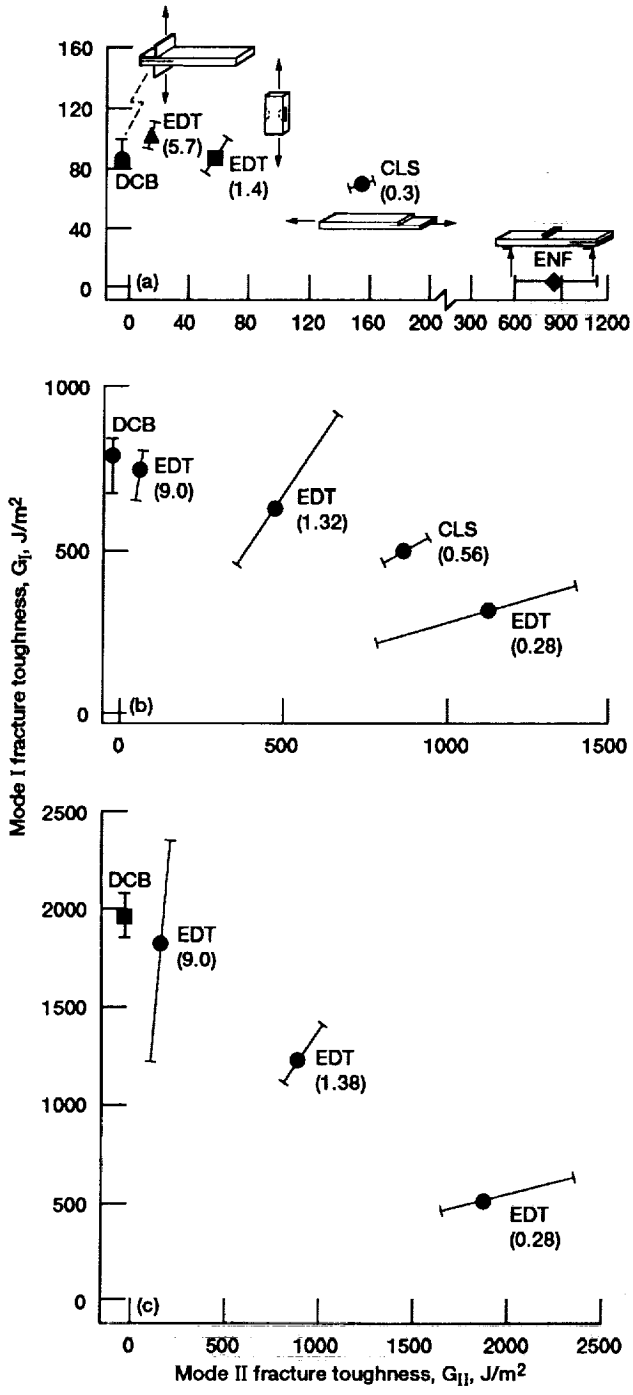

(a) 5208 Epoxy matrix composites.
(b) Hx205 Epoxy matrix composites.
(c) F-185 Epoxy matrix composites.

Figure 31.—Interlaminar fracture toughness depends on crack propagation mode and matrix toughness(adapted from ref. 39). CLS = clapped-lap shear test; EDT = edge-delamination tension test; DCB = double cantilever beam test: ENF = end-notched flexure test.

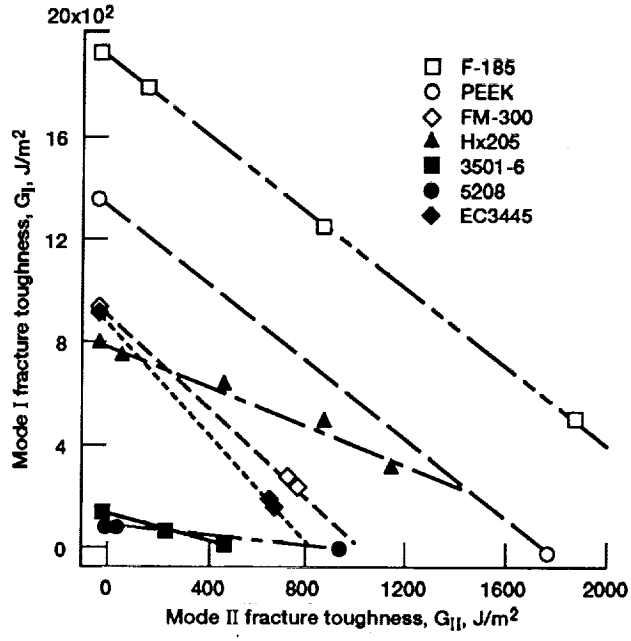

Figure 32.—Fracture toughness calculated with linear mixed-mode failure criterion (adapted from ref. 39).

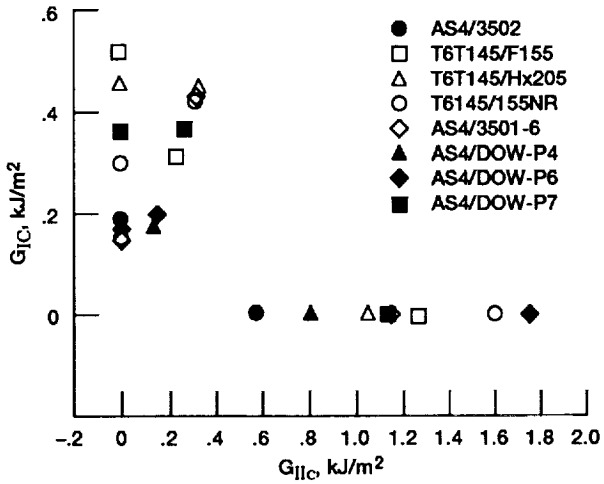

Figure 33.—Interlaminar fracture toughness test data (adapted from ref. 28).

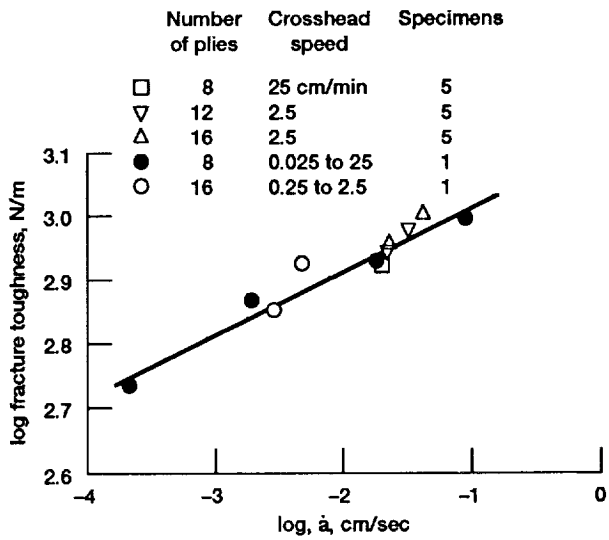

Figure 34.—Energy release rate varies with crack speed for E-glass/epoxy DCB test (adapted from ref. 10).

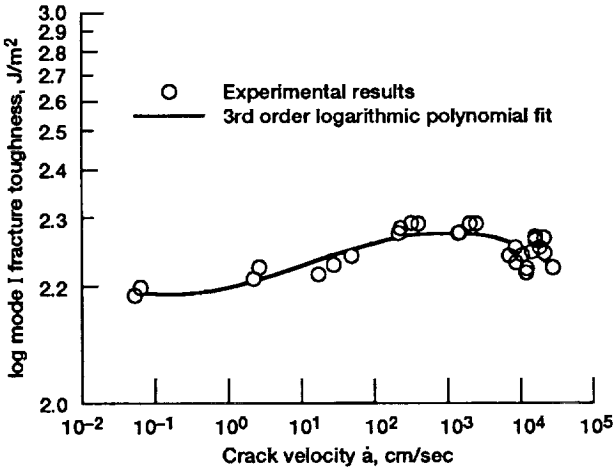

Figure 35—Mode I toughness varies with crack speed for AS4/3501-6 composite (adapted from ref. 19).

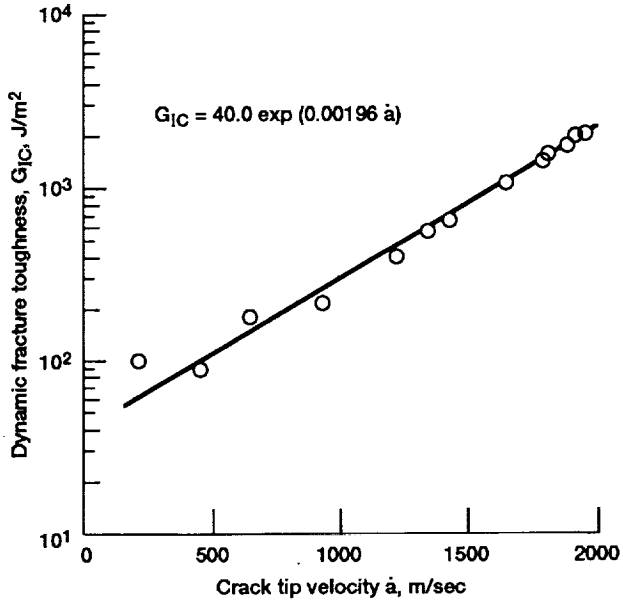

Figure 36—Mode I toughness for AS4/3501-6 at high crack speeds (adapted from ref. 69).

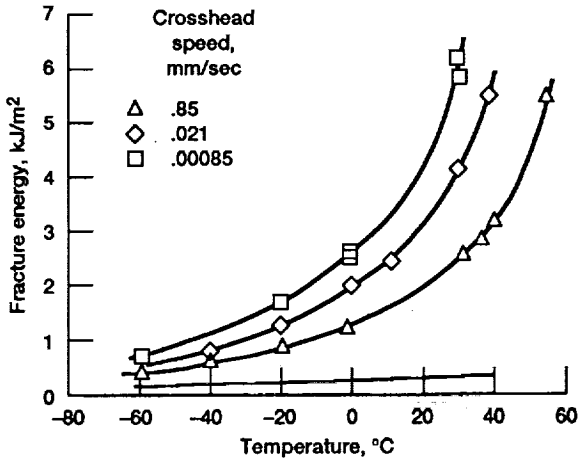

Figure 37.—Fracture energy of a toughened epoxy varies with temperature and loading rate (adapted from ref. 71).

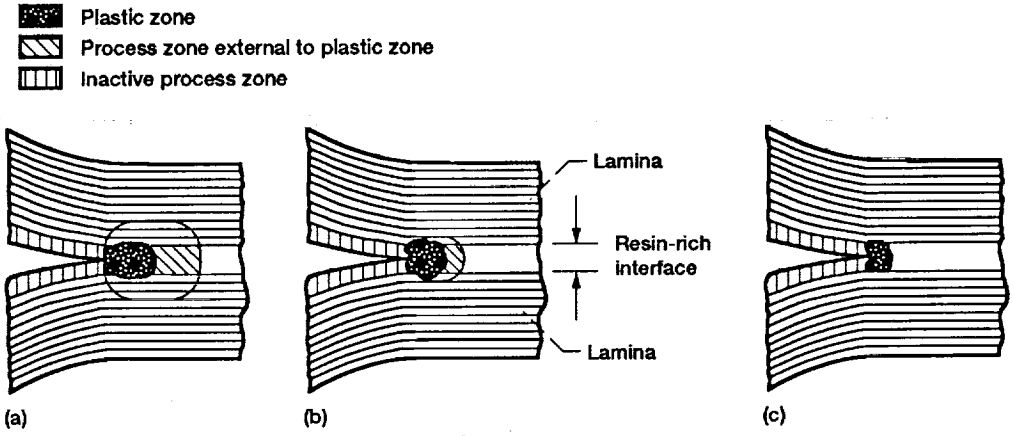

(a) Low loading rates.
(b) Intermediate loading rates.
(c) High loading rates.

Figure 38.—Crack-tip process zone development (adapted from ref. 11).

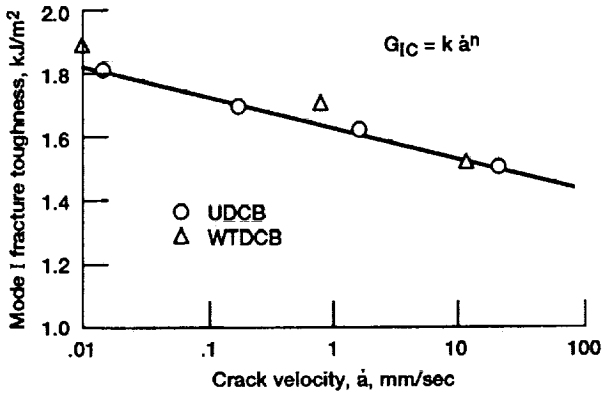

Figure 39.—T300/F-185 fracture toughness decreases with loading rate (adapted from ref. 8). k = 1.625, n = 0.0271.

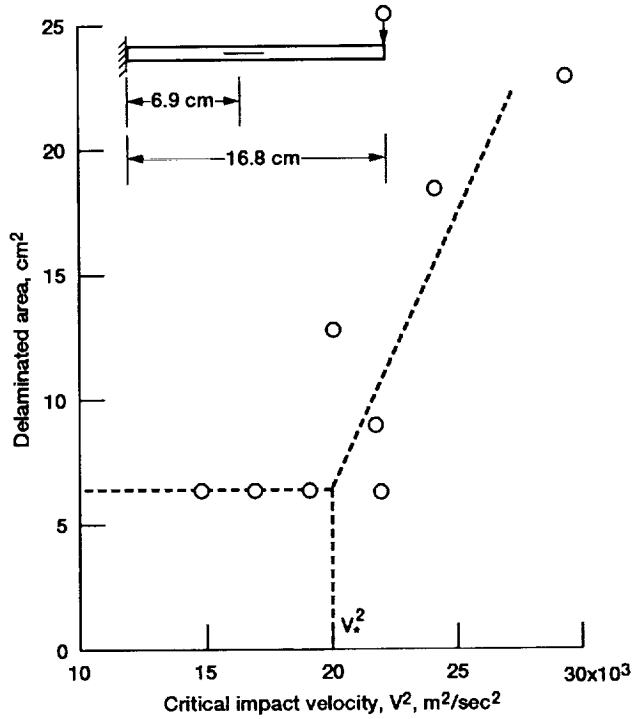

Figure 40.—Critical impact velocity (V_*) is determined from post-impact measurements of delamination length (adapted from ref. 73).

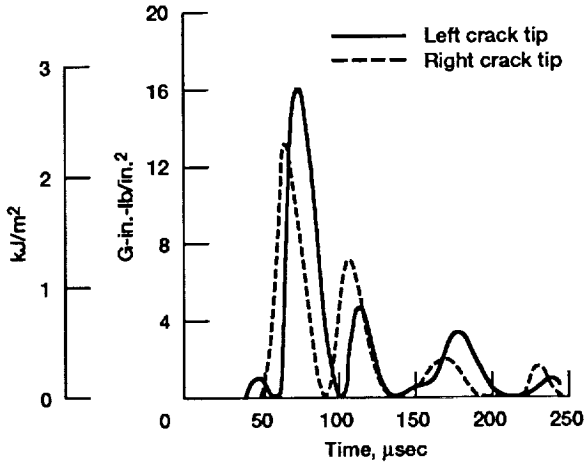

Figure 41.—G_{IIc} is calculated from finite element analysis of impact test (adapted from ref. 74).

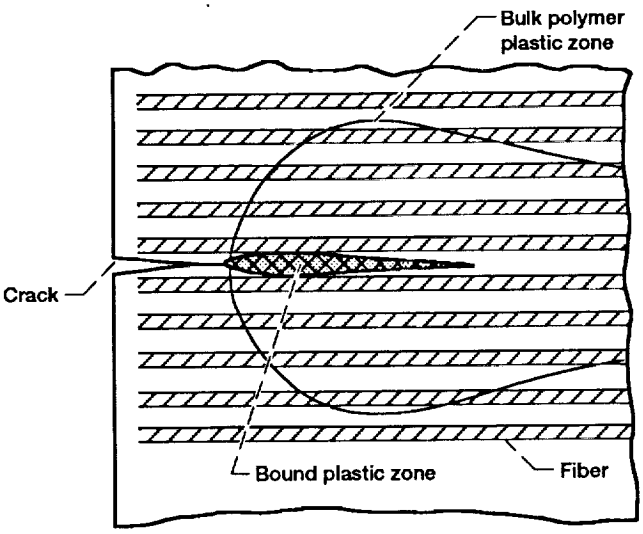

Figure 42.—Fibers restrict development of crack tip plastic zone (adapted from ref. 77).

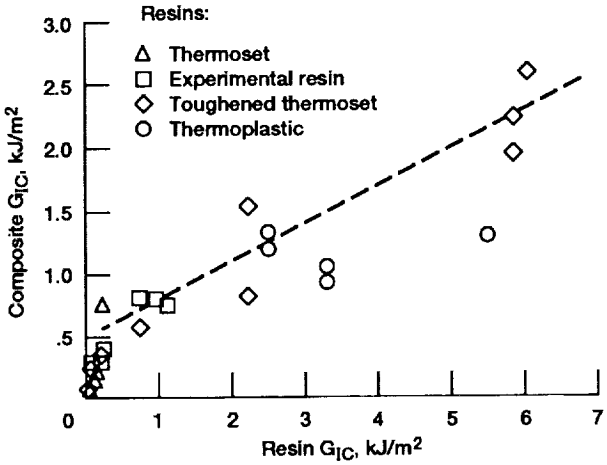

Figure 43.—Strain energy release rates for steady interlaminar crack growth versus neat resin toughness (adapted from ref. 30).

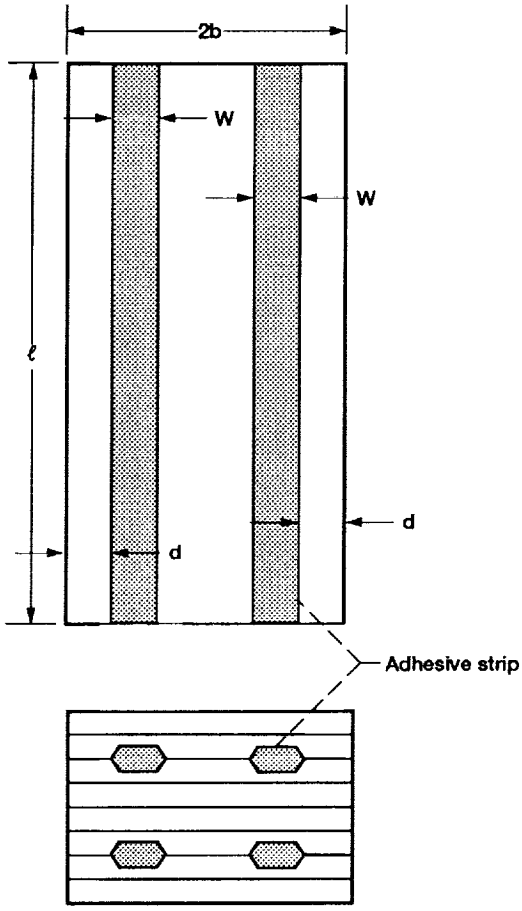

Figure 44.—Location of adhesive interply layers in AS4/3501-6 laminate (adapted from ref. 84).

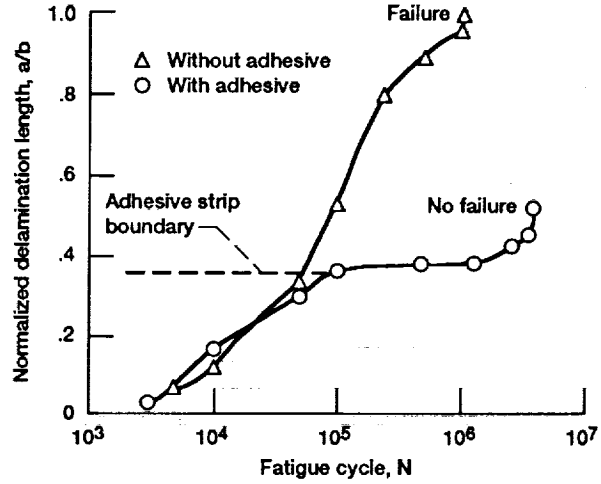

Figure 45.—Adhesive interply layer arrests delamination growth due to fatigue loading (adapted from ref. 84).

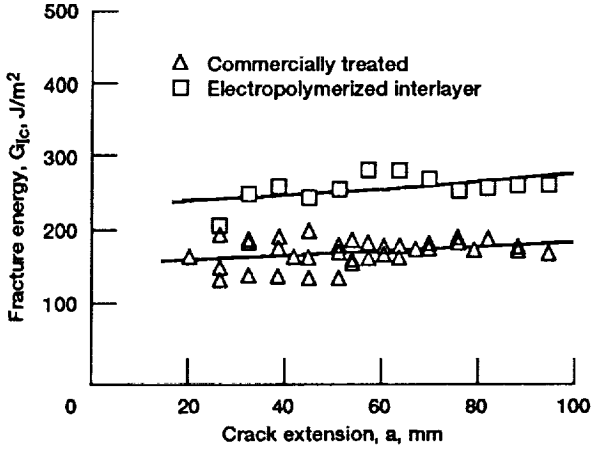

Figure 46.—Increase in G_{Ic} due to electropolymerized interlayer on fiber surface (adapted form ref. 88).

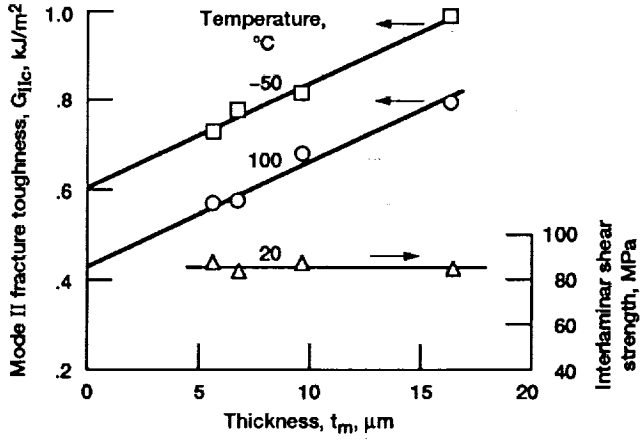

Figure 47.—Increase in G_{IIc} due to thickness of resin-rich interply layer (adapted from ref. 24).

REPORT DOCUMENTATION PAGE

Form Approved
OMB No. 0704 0188

1. AGENCY USE ONLY (*Leave blank*)	2. REPORT DATE	3. REPORT TYPE AND DATES COVERED
	November 1992	Technical Paper

4. TITLE AND SUBTITLE

Fracture Toughness Testing of Polymer Matrix Composites

5. FUNDING NUMBERS

WU–505–63–1B

6. AUTHOR(S)

Joseph E. Grady

7. PERFORMING ORGANIZATION NAME(S) AND ADDRESS(ES)

National Aeronautics and Space Administration
Lewis Research Center
Cleveland, Ohio 44135–3191

8. PERFORMING ORGANIZATION REPORT NUMBER

E-6455

9. SPONSORING/MONITORING AGENCY NAMES(S) AND ADDRESS(ES)

National Aeronautics and Space Administration
Washington, D.C. 20546–0001

10. SPONSORING/MONITORING AGENCY REPORT NUMBER

NASA TP–3199

11. SUPPLEMENTARY NOTES

Responsible person, Joseph E. Grady, (216) 433–6728.

12a. DISTRIBUTION/AVAILABILITY STATEMENT

Unclassified/Unlimited
Subject Category 24

12b. DISTRIBUTION CODE

13. ABSTRACT (*Maximum 200 words*)

A review of the interlaminar fracture literature indicates that a standard specimen geometry is needed to obtain consistent fracture toughness measurements in polymer matrix composites. In general, the variability of measured toughness values increases as the toughness of the material increases. This variability could be caused by incorrect sizing of test specimens and/or inconsistent data reduction procedures. A standard data reduction procedure is therefore needed as well, particularly for the tougher materials. Little work has been reported on the effects of fiber orientation, fiber architecture, fiber surface treatment on interlaminar fracture toughness, and the mechanisms by which the fibers increase fracture toughness are not well understood. The little data that is available indicates that woven fiber reinforcement and fiber sizings can significantly increase interlaminar fracture toughness.

14. SUBJECT TERMS	15. NUMBER OF PAGES
Composite materials; Fracture; Toughness; Test methods	36
	16. PRICE CODE A03

17. SECURITY CLASSIFICATION OF REPORT	18. SECURITY CLASSIFICATION OF THIS PAGE	19. SECURITY CLASSIFICATION OF ABSTRACT	20. LIMITATION OF ABSTRACT
Unclassified	Unclassified		

NSN 7540-01-280-5500

Standard Form 298 (Rev. 2-89)
Prescribed by ANSI Std. Z39-18

NASA-Langley, 1992